Prkra is the double-stranded RNA sensor to mediate an embryonic integrated stress response

Tong Lu[1], Pengcheng Ma[2], Aijun Chen[1], Hailing Fang[1], Jianlin Xu[2], Mingyu Wang[3], Ling Su[1], Sen Wang[3], Yizhuang Zhang[1], Jiasheng Wang[1], Boya Yang[1], De-Li Shi[4], Yong Zhou[5], Qianqian Gong[1], Xiangguo Liu[1,7]*, Bingyu Mao[2]*, Ming Shao[1,6,7]*

[1]Shandong Provincial Key Laboratory of Animal Cell and Developmental Biology and Key Laboratory for Experimental Teratology of the Ministry of Education, School of Life Sciences, Shandong University, Qingdao 266237, China;
[2]State Key Laboratory of Genetic Resources and Evolution, Kunming Institute of Zoology, Chinese Academy of Sciences, Kunming 650223, China;
[3]State Key Laboratory of Microbial Technology, Institute of Microbial Technology, Qingdao 266237, China;
[4]Developmental Biology Laboratory, CNRS-UMR7622, Institut de Biologie Paris-Seine, Sorbonne University, Paris 75005, France;
[5]Yangtze River Fisheries Research Institute, Chinese Academy of Fishery Sciences, Wuhan 430223, China;
[6]Qilu Hospital (Qingdao), Cheeloo College of Medicine, Shandong University, 758 Hefei Road, Qingdao, Shandong, 266035, China;
[7]Shandong University-Yuanchen Joint Biomedical Technology Laboratory, Qingdao, 266237, China.

*Correspondence: xgliu@sdu.edu.cn (X.G.L.), mao@mail.kiz.ac.cn (B.Y.M.); shaoming@sdu.edu.cn (M.S.)

Graphical abstract

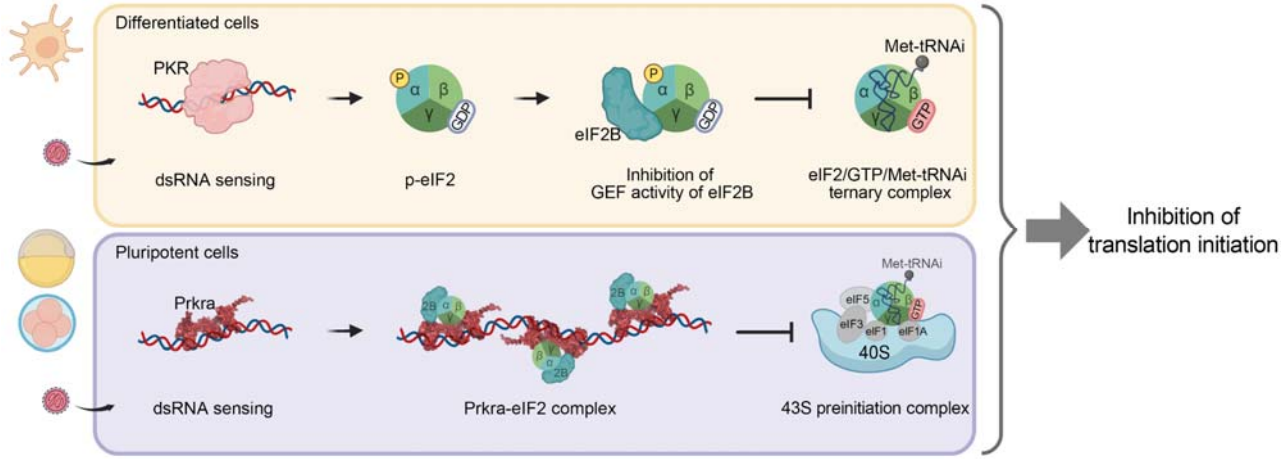

Text Abstract

Nucleic acid sensing, the initial stage of pathogen detection, plays a fundamental role in innate immunity. Double-stranded RNAs, mainly of viral origin, are recognized by protein kinase R (PKR/Eif2ak2) in differentiated cells to trigger an integrated stress response (ISR), characterized by the inhibition of global translation. However, in pluripotent cells, the sensor of double-stranded RNAs in antiviral innate immunity is poorly defined and conflated with those in differentiated cells. In this study, we utilized early zebrafish embryos as a model for pluripotent cells and discovered that dsRNA stimulation induces cell necrosis and a PKR-independent blockage of translation initiation. We identified Prkra as the genuine dsRNA sensor in this unique embryonic ISR. Prkra binds to and polymerizes on dsRNAs, diverting the eIF2 complex away from the translation machinery. Consequently, the formation of the 43S preinitiation complex is significantly reduced, leading to a hindrance in global protein synthesis. This distinctive embryonic ISR not only restricts RNA virus SVCV replication in zebrafish embryos but also exhibits conservation in early mouse embryos and embryonic stem cells. Therefore, the Prkra-mediated translation blockage potentially represents a common antiviral strategy across species.

Keywords

Double-stranded RNA; Prkra; dsRNA sensor; integrated stress response; early embryos; embryonic stem cells

Introduction

Double-stranded RNA (dsRNA) is an evolutionarily conserved pathogen-associated molecular pattern that frequently accumulates during viral infections due to viral genome replication (1-3). Detection of dsRNA serves as a fundamental innate immune defense mechanism in many organisms. In particular, dsRNAs trigger an integrated stress response (ISR) characterized by a global inhibition of translation (4-6). This response is initiated by the activation of the dsRNA sensor protein kinase R (PKR), also known as EIF2AK2 (7). Mechanistically, upon stimulation by dsRNA, PKR phosphorylates the Ser^{51} of eIF2α, a subunit of translation initiation factor eIF2. This phosphorylation transforms eIF2 from a substrate into an inhibitor of the guanine nucleotide exchange factor eIF2B (8,9). As a result, the conversion of inactive eIF2-GDP to its active form, eIF2-GTP, is impeded. Consequently, the formation of the eIF2 ternary complex and the 43S preinitiation complex, both of which are instrumental in initiating the translation of AUG-started open reading frames, is blocked (10). The dsRNA-induced ISR is generally regarded as a part of the antiviral innate immune mechanism that directly inhibits viral protein synthesis (11-13). However, since these insights and concepts have been established primarily in differentiated cells, their full applicability to pluripotent stem cells remains unknown.

Accumulating evidence indicates that there are significant differences in the response of undifferentiated and terminally differentiated cells to virus and dsRNA stimulation. In contrast to most cell types, pluripotent embryonic stem cells (ESCs) and embryonic carcinoma cells do not produce type I interferons (IFNs) in response to viral infection or poly(I:C) treatment (14). In addition, these cells show weak responses to exogenous IFN (15), suggesting that pluripotent cells do not primarily rely on canonical IFN signaling for antiviral activity. Instead, a panel of intrinsically expressed Interferon Stimulated Genes (ISGs) safeguards stem cells against viral infections, with PKR being notably absent from this panel (16). Furthermore, the expression of PKR in zebrafish early embryos is found to be extremely low (17), which raises questions regarding its involvement in translational control at the early stage of development. Hence, it is plausible that undifferentiated cells employ unique mechanisms for dsRNA recognition and translation regulation, which may not rely on the PKR-eIF2α axis typically observed in differentiated cells.

Using zebrafish early embryos as a model of pluripotent cells, we discovered that dsRNAs trigger a distinct stress response characterized by cell necrosis and inhibition of translation. Contrary to expectations, we found that the classic players PKR and phosphorylated eIF2α do not contribute to this ISR-like phenomenon. Instead, we have identified Prkra as a conserved dsRNA sensor, playing a crucial role in this unique ISR-like event observed in early embryos of both zebrafish and mice, as well as in mouse embryonic stem cells (ESCs). In contrast to eIF2α phosphorylation, Prkra mediates global inhibition of translation by directly sequestering the eIF2 complex away from the translation machinery. Therefore, our work has uncovered a shared antiviral mechanism that specifically operates in undifferentiated cells.

Materials and Methods

Reagents and Resources

REAGENT or RESOURCE	SOURCE	IDENTIFIER
Antibodies		
Mouse monoclonal anti-α-tubulin	HUAbio	Cat. #EM0103
Mouse monoclonal anti-GFP	Roche	Cat. #11814460001
Mouse monoclonal anti-His-tag	Beyotime	Cat. #AF2876
Mouse monoclonal anti-β-actin	Proteintech	Cat. #66009-1-Ig
Mouse monoclonal anti-J2	Scicons	Cat. #10010500
Mouse monoclonal anti-Myc (9E10)	Abcam	Cat. #ab32
Mouse monoclonal anti-puromycin	EMD Millipore	Cat. #MABE343
Rabbit polyclonal anti-Rpl10a	Abcam	Cat. #ab174318
Rabbit polyclonal anti-Rps3	Abcam	Cat. #ab128995
Rabbit polyclonal anti-PACT(prkra)	Proteintech	Cat. #10771-1-AP
Rabbit polyclonal anti-eIF2α	CST	Cat. #5324S
Rabbit polyclonal anti-p-eIF2α (S51)	CST	Cat. #9721S
Bacterial Strains		
Escherichia coli DH5α		
Escherichia coli Top10		
Escherichia coli Roseta		
Chemicals, Peptides, and Recombinant Proteins		
GenCrispr NLS-Cas9-NLS nuclease	GenScript	Cat. #Z03389
ActinGreen™ 488 ReadyProbes™ reagent (phalloidin)	Invitrogen	Cat. #R37110
Cycloheximide	Mdbio	Cat. #101-66-81-9
dextran, Alexa Fluor® 647; 10000 MW, anionic, fixable	Life Technologies	Cat. #D22914
Hoechst stain 33342	CST	Cat. #4082S
PI	Thermo Fisher	Cat. #P1304MP
0.25% Trypsin-EDTA (1x)	Gibco	Cat. #25200-056
SeaPlaque® GTG® agarose	Genetic Technology Grade	Cat. #50112
2× M5 HiPer SYBR premix	MF787-01	Cat. #Mei5
DIG RNA labeling mix	Roche	Cat. #11277073910
PEG-8000	SIGMA	Cat. #89510-250-F
T5 exonuclease	NEB	Cat. #M0663S
PhosSTOP	Roche	Cat. #4906845001
Pronase	Roche	Cat. #PRON-RO
Puromycin	Solarbio	Cat. #P8230
Terminator™ 5'-phosphate-dependent exonuclease	LUcigen	Cat. #TER51020
Nitrocellulose blotting membrane	Amersham	Cat. #10600003
Hybond™-N nylon membrane optimized for nucleic acid transfer	Amersham	Cat. #S952
Ni column	Bestchrom	Cat. #AA0051

Dyna Protein G beads	Invitrogen	Cat. #10004D
Cap analog	NEB	Cat. #S1407S
SP6 RNA polymerase	NEB	Cat. #M0207S
T7 RNA polymerase	NEB	Cat. #M0251S
T4 PNK	NEB	Cat. #M0201S
T4 RNA ligase 2	NEB	Cat. #M0242S
SuperScript III	Invitrogen	Cat. #18080-093
CircLigase	Epicentre	Cat. #CL4111K
RNA Inhibitor	Thermo Fisher	Cat. #EO0381
RNase I	Invitrogen	Cat. #AM2294
Dnase I recombinant, Rnase-free	Roche	Cat. #4716728001
Cellulose	Sigma-Aldrich	Cat. #C6288
Critical Commercial Assays		
mMESSAGE mMACHINE T7	Ambion	Cat. #AM1344
mMESSAGE mMACHINE SP6	Ambion	Cat. #AM1340
Dual luciferase reporter gene assay kit	YEASEN	Cat. #11402ES60
TransScript First-Strand cDNA Synthesis Kit	Transgene	Cat. #AT301
JB-4 embedding kit	Sigma	Cat. #EM0100-1KT
Magnetic RNA-protein pulldown kit	Thermo Fisher	Cat. #20164Y
Silver staining kit	Beyotime	Cat. #P0017S
Chemiluminescent nucleic acid detection module	Thermo Fisher	Cat. #89880
Ezup column animal genomic DNA purification kit	Sangon Biotech	Cat. #B518251-0050
Experimental Models: Transgenic or Mutant Strain		
Zebrafish AB wide-type	This paper	N/A
Zebrafish MZ*eif2ak2* CRISPant	This paper	N/A
Zebrafish MZ*prkra* CRISPant	This paper	N/A
Mouse C57L/B6 type	This paper	N/A
Mouse DBA/2 type	This paper	N/A
Mouse *Prkra* knockout cell line	This paper	N/A
Oligonucleotides		
Sequences of dsRNAs (see Supplementary Table S1)		
Primers (see Supplementary Table S2)		
Recombinant DNAs		
pCS2-*cas9*	This paper	N/A
pCS2-*tol2*	This paper	N/A
pCS2-*nanog*	This paper	N/A
pT2AL200R150G	This paper	N/A
pCS2-GFP	This paper	N/A
pCS2-*luciferase*	This paper	N/A
pCS2-vps26c	This paper	N/A

pCS2-DV	This paper	N/A
pCS2-EBOV	This paper	N/A
pCS2-HIV	This paper	N/A
pCS2-H1N1	This paper	N/A
pCS2-CoV-2	This paper	N/A
pCS2-TILV	This paper	N/A
pCS2-ZIKV	This paper	N/A
pET Duet-prkra WT His	This paper	N/A
pET Duet-prkra Δ123 His	This paper	N/A
Software and Algorithms		
ImageJ	ImageJ	https://imagej.net/
Prism	GraphPad	https://www.adobe.com/
Adobe Premiere Pro CC	Adobe	https://www.graphpad.com/
Chromas	Technelysium	https://technelysium.com.au/wp/
TBtools	Chen et al. (2020)	https://github.com/CJ-Chen/TBtools/
Biorender	Biorender	https://app.biorender.com
ZEN	ZEISS	https://www.zeiss.com/

Animals

Zebrafish AB strain, *eif2ak2* and *prkra* mutant lines were raised in standard breeding systems (Haisheng) at 28 ^{o}C. All experiments followed the ARRIVE guidelines approved by the Ethics Committee for Animal Research of Life Science of Shandong University (permit number SYDWLL-2023-069).

All mice with C57L/B6 and DBA/2 mice backgrounds were kept in individually ventilated cages (IVC) in a specific pathogen-free (SPF) environment and handled according to guidelines approved by the Animal Care and Use Committee of the Kunming Institute of Zoology, Chinese Academy of Sciences (IACUC-RE-2024-05-002).

Generation of zebrafish maternal and zygotic mutants

We adopted a CRISPant strategy to generate zygotic mutants and maternal mutants rapidly (18). sgRNAs targeting the open reading frames (ORFs) of *eif2ak2* and *prkra* were designed by the online tools CRISPRscan (19). They were prepared via standard *in vitro* transcription and purification. The purified sgRNA (100 pg) was injected with Cas9 protein (200 pg) into the fertilized egg. At 10 hpf, embryos were homogenized in 50 mM NaOH for 20 min at 95 ^{o}C followed by the addition of 1/10 volume of 1 M Tris-HCl (pH 7.5). The DNA fragment flanking the sgRNA binding site was PCR amplified and sequenced. Sequencing chromatogram files were submitted to http://shinyapps.datacurators.nl/tide/ to estimate the efficiency of the sgRNA. The adult CRISPant male and female F0 fish were crossed to obtain MZ mutant embryos, which were verified by RT-PCR analysis using cDNAs from 1-cell stage embryos for analysis of maternal transcripts or from shield-stage embryos for analysis of MZ transcripts. The PCR products were also subcloned and subjected to Sanger sequencing.

Mouse embryos and mESC knockout lines

Female C57BL/6 (6-8 weeks old) were induced to superovulation by intraperitoneal injection of 7.5 IU pregnant mare serum gonadotropin (ProSpec, HOR-272) followed by 7.5 IU human chorionic gonadotropin (HCG) (ProSpec, HOR-250) with a 48 hours interval. Immediately after the HCG injection, female mice were housed with DBA/2 male mice for mating. Zygotes were collected from the oviducts and treated with 0.1% hyaluronidase (Sigma, H35056) in an M2 medium (Sigma, M7167) to remove cumulus cells. They were then transferred to KSOM medium (Millipore, MR-106-D) with paraffin oil (Sigma, 18512) at 37 °C

under a 5% CO_2 environment. After injection of 100 pg dsRNAs with/without 50 pg eGFP mRNA into the cytoplasm using a constant flow system (IX73 OLYMPUS and FemtoJet Eppendorf), embryos were cultured in KSOM medium to stage E4.5. The mouse E4.5 ESC line derivation was previously described (20). They were cultured in 2i medium (Millipore ESG1107) supplemented with 15% FBS (GIBCO). Two sgRNAs targeting the *Prkra* locus were introduced into mESCs,(21) and mutant cells were obtained by FACS sorting and expanded to establish stable cell lines. Mutation was confirmed by Sanger sequencing and western blot analysis.

Live imaging

Zebrafish embryos were dechorionated by pronase treatment at a concentration of 1 mg/mL for 10 minutes. They were then embedded in 1.5% low-melting agarose on a petri dish with a glass bottom, and their position was adjusted before agarose solidification. The dish was added with 1/3x Ringer's buffer and placed on an inverse microscope (JiangNan, XD-202) for time-lapse recording. Differential interference contrast (DIC) images were acquired using a Leica upright microscope (Leica, DM2500) by embedding dechorionated embryos in 1.5% low-melting agarose on a concavity slide. Time-lapse videos were edited using Adobe Premiere Pro CC software.

mRNA and dsRNA synthesis

The coding sequences from genes of interest were PCR amplified or directly synthesized and subcloned into the pCS2 vector via a modified Gibson Ligation method (22). Recombinant vectors were linearized by NotI digestion, purified with a PCR cleanup kit, and used as the DNA templates for mRNA synthesis using the mMESSAGE mMACHINE SP6 or T7 kit (Cat. #AM1344 and Cat. #AM1340) according to the manufacturer's instruction. The DNA template was removed by DNase I treatment at 37 ^{o}C for 15 minutes, and synthesized mRNAs were extracted by pheno-chloroform and precipitated by adding an equal volume of ice-cold isopropanol. After centrifugation at 12,000 *g* at 4 ^{o}C for 15 minutes, the pellet was rinsed with 70% cold ethanol and resuspended in 15-20 μL RNase-free water.

Templates for dsRNAs were PCR amplified from plasmids containing the entire ORFs or synthesized directly. T7 and SP6 promoter sequences were added to the 5' or 3' end of the DNA template by incorporating them into the 5' end of amplifying primers. Sense and antisense RNAs were synthesized separately using T7 or SP6 RNA polymerase. They were annealed in a PCR thermocycler with a program of 95 ^{o}C for 5 min, ramping down at 0.1 ^{o}C/s to 50 ^{o}C and quickly cooling to 4 ^{o}C.

Cellulose chromatography

IVT mRNAs (50 μg) were incubated with 50 mg cellulose twice for 30 minutes in a buffer containing 10 mM HEPES (pH 7.2), 0.1 mM EDTA, 125 mM NaCl, and 16% (v/v) ethanol. The mixture was centrifuged at 12,000 g at 4 ^{o}C, and the supernatant was recovered. The RNAs in the supernatant were then precipitated by adding 1/10 volume of 4 M NaAc (pH 4.0) and 2.5 volume of absolute ethanol. After a thorough vortex, the mixture was incubated in a -20 ^{o}C refrigerator for 30 minutes and then centrifuged at 12,000 g for 15 minutes at 4 ^{o}C. The pellet was rinsed in 70% ethanol and resuspended in RNase-free water.

dsRNA detection

Dot blot was used to detect dsRNAs, and the analysis was done using a dsRNA-specific J2 antibody. For dot blot, nylon membrane was spotted with RNAs (200 ng) using a 10 μL pipet tip and incubated with 1/2000 dilution of the dsRNA-specific J2 antibody at 4 ^{o}C for 12 hours. The membrane was washed with TBST thrice for 10 minutes and incubated with anti-mouse IgG-HRP diluted at 1/5000. After washing with TBST thrice for 10 minutes, dsRNAs were visualized using an ECL reagent and a chemiluminescence imaging system (SINSAGE).

Phalloidin, PI, and Hoechst staining

For phalloidin staining, zebrafish embryos were fixed with freshly made 4% paraformaldehyde and washed in PBST thrice for 10 minutes. The embryos were then incubated with phalloidin for 30 minutes and washed in PBST thrice for 10 min. They were analyzed under a confocal microscope (Zeiss LSM880), and Z-stack projections were obtained using the z-projection function of the compatible software ZEN.

For PI and Hoechst staining, live embryos were cultured in E3 buffer containing 1 μg/mL PI and 1 μg/mL Hoechst33342. They were subjected to fluorescence time-lapse imaging under an inverse microscope, or mounted in 1.5% low-melting agarose and imaged under a ZEISS confocal microscope. Cell dissociation was performed by treatment with 0.25% Trypsin-EDTA (m/v) at 37 ^{o}C for 15 minutes and gentle pipetting. Single cells were cultured in E3 buffer containing 1 μg/mL PI and 1 μg/mL Hoechst33342 and subjected to time-lapse analysis using a Leica inverse microscope equipped with the Thunder function (THUNDER DMi8).

Microinjection and cell transplantation

Microinjection was performed using a PLI-100A Picoliter microinjector (Harvard apparatus). A volume of 1-2 nL was injected into the embryo at the 1-cell stage. Cell transplantation experiments were performed as described previously (23). Briefly, WT embryos were first labeled with Alexa-647-dextran. At the high stage, cells in the blastodisc were aspirated using the Picoliter microinjector and injected into the animal pole region of stage-matched recipients. At 6 hpf, chimeric embryos were mounted in 1% low-melting agarose on a coverslip for confocal imaging.

Western blotting

Embryos were dechorionated, and the yolk was removed manually. Cell pellets were collected in 1.5 mL centrifuge tube and lysed in a lysis buffer (100 mM NaCl, 0.5% NP-40, 5 mM EDTA, 10 mM Tris-HCl, pH 7.5) containing protease inhibitors. Samples were boiled in Lammeli buffer (10% SDS, 0.5% bromophenol blue, 50% glycerol, 5% β-Mercaptoethanol, 250 mM Tris-HCl, pH 6.8). Proteins were separated by SDS polyacrylamide gel electrophoresis and transferred to a nitrocellulose membrane. Primary antibodies used for western blot analysis are listed in the key resources Table.

qRT-PCR

Total RNAs were extracted at appropriate stages, and cDNAs were prepared using the TransScript First-Strand cDNA Synthesis Kit (Transgene) following the manufacturer's protocols. qPCR was performed using 2 x M5 HiPer SYBR premix (MF787-01, Mei5) on a Q2000 real-time PCR system (LongGene). Primers used for amplifying genes of interest are listed in Supplementary Table S2. The $2^{-\Delta\Delta Ct}$ method was used to estimate relative expression levels with *gapdh* amplicon as the loading control.

Electron microscopy

Embryos were fixed in 2.5% glutaraldehyde buffered in PBS for 1-4 hours at 4 ^{o}C. After washing in PBS five times for 20 minutes, they were fixed using 1% osmic acid. Following rinse in PBS thrice for 15 minutes, samples were dehydrated through graded ethanol series and treated twice using absolute acetone. They were then infiltrated with epon812 resin and solidified by increasing temperature (12 hours at 36 ^{o}C, 12 hours at 50 ^{o}C, and 24 hours at 60 ^{o}C). Ultrathin sections were prepared using an ultramicrotome (PowerTome-XL) equipped with a glass knife and sectioned at 100 nm thickness. The sections were then stained with 2% uranium acetate and 3% lead citrate and visualized under a focused ion beam scanning electron microscope (ZEISS, crossbeam550).

JB4 sectioning

Embryos were fixed overnight at 4 ^{o}C in PBS-buffered 4% paraformaldehyde. They were embedded in JB-4 resin (Sigma-Aldrich) as suggested by the manufacturer's guide. Sections of 2 μm thickness were obtained using an ultramicrotome (PowerTome-XL) equipped with a glass knife and stained with hematoxylin and hydrophilic eosin Y.

Puromycin incorporation assay

Embryos were treated with 50 μg/mL puromycin from 2 hpf to 4 hpf. They were harvested following removal of yolk cells and lysed in protein IP buffer (10 mM Tris-HCl, pH 8, 150 mM NaCl, 1% NP-40, 1 mM EDTA, 10 μg/mL Aprotinin, 10 μg/mL Leupeptin, and 1 mM PMSF) After denaturation at 95 ^{o}C for 5 minutes, the puromycin-conjugated proteins were visualized by western blot analysis using a puromycin antibody.

Luciferase assay

Synthetic *luciferase* mRNAs (50 pg) were injected alone or coinjected with dsRNA or dsRNA-contaminated mRNAs into 1-cell stage embryos. At 6 hpf, injected embryos (30 at least) were lysed in a passive lysis buffer provided in the Dual-Luciferase Reporter Gene Assay kit. After centrifugation at 12,000 *g* for 10 minutes, the supernatant was mixed with firefly luciferase substrate (50 μL lysate plus 50 μL substrate) and quantified using a luminometer (Berthold, Junior LB 9509).

Sucrose density gradient centrifugation

Sucrose was thoroughly dissolved in polysome buffer (50 mM Tris-HCl, pH 7.0, 100 mM NaCl, 5 mM $MgCl_2$, 100 μg/mL CHX) to prepare 10% and 60% sucrose solutions. The sucrose density gradient was generated in a 41Ti centrifuge tube on a Gradient Station (BIOCOMP) and allowed to equilibrate. Embryos at 5-hpf were collected from controls and dsRNA-injected groups. After removal of the chorions using pronase, embryos were treated with 50 μg/mL CHX for 10 minutes and lysed on ice in lysis buffer (1% Triton X-100, 300 U/mL RNase inhibitor, 10 μg/mL aprotinin, 10 μg/mL leupeptin, and 1 mM PMSF). The lysate was centrifuged at 12,000 *g* for 10 minutes at 4 ^{o}C. The supernatant was carefully loaded onto the top of the sucrose density gradient curtain and centrifuged at 240000 g for 2 hours using an ultracentrifuge (Beckman, XPN-100). Following centrifugation, the centrifuge tube was loaded onto a density fractionation system (BIOCOMP), which was utilized to separate the fractions and measure the absorbance at 260 nm. A 10 kDa ultrafiltration tube (Millipore) was used to concentrate proteins according to the manufacturer's instructions.

Ribosome profiling and bioinformatic analysis

This was performed by following established experimental procedures with modifications (24). Briefly, both control and dsRNA-injected embryos at 5 hpf were thoroughly lysed on ice in lysis buffer (20 mM Tris-HCl, pH 7.4; 150 mM NaCl; 5 mM $MgCl_2$; 1 mM DTT; 100 μg/ml CHX; 1% Triton X-100 and 25 U/mL Turbo DNase I). The lysate was centrifuged at 12,000 *g*, 4°C for 10 minutes to remove cell debris. The supernatant was added with 0.2 U/μL RNase I and incubated at 25 °C for 30 minutes to digest free RNAs unprotected by ribosomes. The digestion was terminated by adding 0.67 U/μL RNase inhibitor. The lysate was then subjected to sucrose density gradient centrifugation, and fractions with a single absorbance peak at 260 nm, corresponding to the 80S monosome, were collected and thoroughly lysed in TRIzol for RNA extraction. RNA fragments within the size of 26-34 nt were separated by denaturing polyacrylamide gel electrophoresis, and desired bands were recovered in RNA elution buffer (300 mM sodium acetate, pH 5.5, 1 mM EDTA, 0.25% SDS). Eluted RNAs were dephosphorylated by T4 PNK and subjected to ligation reaction using T4 RNA ligase 2, to add a preadenylylated and 3'-blocked linker (5' rApp-CTGTAGGCACCATCAAT-NH_2 3') at the 3' end. The RNA fragments with linker were extracted and reverse transcribed using SuperScript III in the presence of the primer 5' (Phos)-AGATCGGAAGAGCGTCGTGTAGGGAAAGAGTGTAGATCTCGGTGGTCGC-(SpC18)-CACTCA-(SpC18)-TTCAGACGTGTGCTCTTCCGATCTATTGATGGTGCCTACAG-3' to obtain extended cDNA molecules. Purified cDNAs were subjected to circularization using CircLigase, forming circular cDNA molecules. To remove residual rRNA components in the cDNAs, we adopted a method involving hybridization with biotinylated rRNA-depletion oligo primers specific to zebrafish rRNAs (GGGGGGATGCGTGCATTTATCAGATCA, TTGGTGACTCTAGATAACCTCGGGCCGATCGCACG, GAGCCGCCTGGATACCGCAGCTAGGAATAATGGAAT, TCGTGGGGGGCCCAAGTCCTTCTGATCGAGGCCC, GCACTCGCCGAATCCCGGGGCCGAGGGAGCGA, GGGGCCGGGCCGCCCCTCCCACGGCGCG, GGGGCCGGGCCACCCCTCCCACGGCGCG, CCCAGTGCGCCCCGGGCGTCGTCGCGCCGTCGGGTCCCGGG, TCCGCCGAGGGCGCACCACCGGCCCGTCTCGCC, AGGGGCTCTCGCTTCTGGCGCCAAGCGT, GAGCCTCGGTTGGCCCCGGATAGCCGGGTCCCCGT, GAGCCTCGGTTGGCCTCGGATAGCCGGTCCCCCGC, TCGCTGCGATCTATTGAAAGTCAGCCCTCGACACA, TCCTCCCGGGGCTACGCCTGTCTGAGCGTCGCT). The remaining circularized cDNAs were amplified through PCR using forward library primer (5'-AATGATACGGCGACCACCGAGATCTACAC-3') and reverse indexed primer (5'-

CAAGCAGAAGACGGCATACGAGATNNNNNNGTGACTGGAGTTCAGACGTGTGCTCTTCCG -3', with NNNNNN representing the reverse complementary sequence of the barcode). The amplified products were separated and recovered using polyacrylamide gel electrophoresis with TE buffer. Subsequently, the library was subjected to quality control assessment, and Illumina Novaseq 6000 S4 (PE150) sequencing was performed to obtain the sequences of ribosome-protected RNA fragments.

Cutadapt was utilized for removing adapters and low-quality reads; Bowtie2 was employed for data mapping and Samtools was used to remove duplicated reads in mapped RNA-seq data (25-27). Self-written scripts were utilized to read and count Ribo-seq and RNA-seq mapping data, analyze RPF position and ribosome density, and visualize the results.

Transcriptome and annotation data were downloaded from NCBI (GCF_000002035.6_GRCz11_rna_from_genomic.fna, GCF_000002035.6_GRCz11_genomic.gtf). The non-coding RNA and mRNA sequence datasets are manually extracted from the downloaded FASTA files.

For Ribo-seq data, adapters and low-quality bases were removed from reads using the cutadapt arguments' -a ACGACGCTCTTCCGATCT...CTGTAGGCACCATCAATAGATCGG -A ATTGATGGTGCCTACAG...AGATCGGAAGAGCGTCG -q 15,10'; reads lengths less than 20 nt or greater than 40 nt after adapter cutting were removed using cutadapt arguments '--minimum-length 20 --maximum-length 40'. For RNA-seq data, adapters, low-quality bases and Ns were removed from the reads using the cutadapt arguments' -a AGATCGGAAGAGCACACG -A AGATCGGAAGAGCGTCGT -q 15,10 --trim-n'; reads length less than 50 nt after adapter cutting were removed using cutadapt argument '--minimum-length 50'.

The clean data of forward reads from Ribo-seq was mapped to non-coding RNA data using Bowtie2 with the arguments "--un unmapped. fasta -k 3", and unmapped reads were subsequently mapped to mRNAs using the arguments "-k 3" to generate the SAM file. Reads mapped to multiple genes were assigned randomly, with probabilities proportional to the number of unique reads associated with each gene. Reads mapped to multiple gene IDs with the same gene name were assigned to the gene ID with the highest number of unique reads. Finally, the reads mapped to multiple transcripts with the same gene ID were assigned to the transcript with the highest number of unique reads.

The clean RNA-seq data were mapped to the transcriptome using Bowtie2 with the argument "-k 3". Duplicated reads were removed from the mapped data using Samtools with the commands: 'samtools fixmate -m; samtools sort; samtools markdup; samtools sort'. Read mapped to multiple gene names, gene IDs, and transcript IDs were handled using the same strategy described for mapping Ribo-seq reads.

The position of RPFs/read on the transcript was determined by the position of the 5' end of the read. The positions of codons on the transcript were identified using the position of the first nt relative to the 5' end of the transcript, with the first nt being designated as position 1. The relative position of a read to the start or stop codon was calculated by subtracting the position of the start or stop codon from the position of the read, respectively. The number of reads relative to the start codon ranging from -24 to 24 nt was counted. In addition, the number of reads was counted relative to the stop codon, ranging from -36 to 12 nt. The number of reads was visualized in a bar plot, and the frame of a read was determined by the remainder by dividing its relative position to the start codon by 3. Subsequently, the fraction of reads, with relative positions to start codon ranging from -12 to 72 nt, that fall into different frames was calculated and visualized in another bar plot.

Reads with relative positions to the start codon between -100 and 300 nt and relative positions to the stop codon between -300 and 100 nt were counted. Only transcripts with CDSs longer than 600 nt were considered during the analysis. A distribution of the number of reads along the mRNA was plotted.

For ribosome density analysis, the following formula is employed:(28)

$$Ribosome_Density = \frac{RPFs_Ribo_seq}{Reads_count_RNA_seq}$$

The sum of RPF/Read count data was scaled to 1e6 to mitigate the effects of sequencing depth. The ribosome density was calculated for genes only with a read count exceeding 64.

Given that the injection of dsRNAs alters the overall translational activity, as demonstrated by the puromycin incorporation experiments, a correction factor was introduced to accommodate this alteration

(0.5 for low-dose dsRNA injection; 0.3 for high-dose injection). The ribosome density of the dsRNA-injected group was multiplied by this factor to reflect the overall translational change in the treatment. Fold changes in ribosome number (the RPF number) after dsRNA stimulation indicate protein synthesis rate. The ribosome number of the treatment group was also multiplied by the correction factor.

GO analysis was performed using tools provided in DAVID Bioinformatics (https://david.ncifcrf.gov/tools.jsp) (29), using all genes with RPF read counts of more than 64 as the background.

RNA pulldown

A detailed protocol is provided in the manual of the Pierce™ Magnetic RNA-Protein Pulldown kit. In general, 50 μL of streptavidin magnetic beads were transferred to RNase-free centrifuge tubes. The tubes were placed on a magnetic separation stand for 30 seconds, and the supernatant was removed. The beads were washed twice with 20 mM Tris-HCl, pH 7.5 (50 μL for each sample). After adding 1x RNA Capture Buffer, the beads were vortexed and incubated with 50 pmol of biotin-labeled RNAs under gentle rotation at room temperature for 20 minutes. The supernatant was removed, and the beads were washed twice with 20 mM Tris-HCl, pH 7.5. In parallel, embryos were lysed in protein lysis buffer (10 mM Tris-HCl, pH 8, 150 mM NaCl, 1% NP-40, 1 mM EDTA, 10 μg/mL aprotinin, 10 μg/mL leupeptin, and 1 mM PMSF). After centrifugation at 12,000 *g* for 10 minutes at 4 ^{o}C, the cleared supernatant was added with a Master Mix containing 1 x protein-RNA binding buffer and 15% glycerol, which was then incubated with the beads at 4 ^{o}C under rotation for 1 hour. Following this incubation, the beads were washed twice with 100 μL 1 x washing buffer with gentle mixing. Finally, the beads were incubated with 50 μL of elution buffer at 37 ^{o}C for 20 minutes. The eluent was subjected to mass spectrum and western blot analyses.

Mass Spectrometry

After RNA pulldown, the samples were subjected to polyacrylamide gel electrophoresis to separate the proteins. To visualize proteins, the gel was stained using a silver staining kit. The silver-stained proteins in each lane were then excised into four parts as independent samples with different molecular weights. Protein digestion was carried out using trypsin following the filter-aided sample preparation (FASP). Digested peptides obtained from each sample were desalted using 3 mL of Empore™ SPE Cartridges C18 (standard density, bed I.D. 7 mm; Sigma-Aldrich). Subsequently, they were concentrated using vacuum centrifugation and reconstituted in 40 μL of 0.1% (v/v) formic acid. LC-MS/MS analysis was conducted using a timsTOF Pro mass spectrometer (Bruker) coupled to Nanoelute (Bruker). The peptides were loaded onto a C18 reversed-phase analytical column (Thermo Scientific Easy Column, 25 cm long, 75 μm inner diameter, 1.9 μm resin) with 95% buffer A (0.1% formic acid in water) and separated using a linear gradient of buffer B (99.9% acetonitrile and 0.1% formic acid) at a flow rate of 300 nL/minute. The mass spectrometer operated in positive ion mode with an applied electrospray voltage of 1.5 kV. Precursor ions and fragments were analyzed using the TOF detector within a mass range of m/z 100-1700. The timsTOF Pro operated in parallel accumulation serial fragmentation (PASEF) mode, with PASEF data collection performed under the following parameters: ion mobility coefficient (1/K0) ranging from 0.6 to 1.6 Vs cm2; 1 MS scan and 10 MS/MS PASEF scans were acquired. Active exclusion was enabled with a release time of 24 seconds.

Two negative controls (RNA-free beads and ssRNAs) were included to set up a stringent strategy for screening dsRNA-associated proteins. The criteria for identifying a specific dsRNA-associated protein are as follows: relative intensity (RI) for dsRNA pulldown (RI_{dsRNA}) should be greater than 10e-4, the ratio of RI for dsRNA (RI_{dsRNA}) to RI for ssRNA (RI_{ssRNA}) should be greater than 3, and the ratio of RI for beads (RI_{beads}) to the average RI of dsRNA and ssRNA ($(RI_{dsRNA}+RI_{ssRNA})/2$) should be less than 0.2. Here, RI is defined as the total intensity of a specific protein divided by the sum of the intensity of all detected proteins. Scatter plot was generated with the horizontal axis representing RI_{dsRNA}, while the vertical axis representing the enrichment index defined as $\log_{10}(1/(RI_{ssRNA}/RI_{dsRNA}+0.01))$. Specific dsRNA-associated proteins were marked in red, whereas grey dots designate proteins with $RI_{dsRNA}/RI_{ssRNA} \leqq 3$ and $RI_{beads}/((RI_{dsRNA}+RI_{ssRNA})/2)<0.2$, and grey circles stand for proteins with $RI_{beads}/((RI_{dsRNA}+RI_{ssRNA})/2) \geqq 0.2$.

Recombinant protein expression and purification

The pET-Duet plasmid was linearized using KpnI and NcoI. A 6 x His tag sequence was inserted at the 3' end in the coding regions of *prkra* or its mutant. The *rossta* strain of *E. coli* transformed with plasmids was cultivated overnight at 37 ^{o}C in LB and inoculated to 1 liter fresh LB for amplification until reaching 0.6 OD (optical density). To induce protein expression, IPTG (1 mM, final concentration) was added to the culture for another 26 hours at 20 ^{o}C with agitation. The bacteria were then harvested by centrifugation at 2800 g for 10 minutes at 4 ^{o}C, and 10% glycerol was used to resuspend the pellets, followed by centrifugation at 1850 g for 20 minutes at 4 ^{o}C. Cell pellets were weighed and resuspended in AP buffer (50 mM Tris-HCl, pH 7.2, 400 mM NaCl, 40 mM imidazole, 10% glycerol, and 0.02% NP-40). Cells were homogenized using lysozyme solution (1 mM DTT, 1 mM PMSF, and 1 mg/mL lysozyme in AP buffer), and sonication was performed using an ultrasonic homogenizer (JY92-IIN) with the program: 5 seconds ON and 10 seconds OFF cycle for 4 minutes, with power setting 20%. After centrifugation at 24,000 g at 4 ^{o}C for 1 hour, the supernatant was filtered using a 0.45 μm membrane. In parallel, the Ni column was prepared and washed twice with ddH_2O, followed by one wash with AP buffer. The cleared supernatant was added to the column and incubated at 4 ^{o}C for 1 hour to allow protein binding. The column was then drained and washed twice with buffer A (1 mM DTT and 1 mM PMSF in AP buffer), followed by the addition of cold buffer B (2 mM ATP-Na, 1 mM MgAc, 1 mM DTT, and 1 mM PMSF in AP buffer) and incubation at 4 ^{o}C for 10 minutes to activate the protein. After two washes with buffer C (1 mM DTT in AP buffer), proteins were slowly eluted with the elution buffer (50 mM Tris-HCl, pH 7.2, 400 mM NaCl, 400 mM imidazole, 10% glycerol, and 0.02% NP-40). For long-term storage, glycerol was added to the proteins at a final concentration of 50% and stored at -80 ^{o}C.

EMSA assay

Biotin-labeled 139 bp RNA was from *Vpr* gene of HIV-1 with the sequence: UCCUAGGAUUUGGCUCCAUGGCUUAGGGCAACAUAUCUAUGAAACUUAUGGGGAUACUUG GGCAGGAGUGGAAGCCAUAAUAAGAAUUCUGCAACAACUGCUGUUUAUCCAUUUCAGAAU UGGGUGUCGACAUAGCAGA. Forward RNA strands were *in vitro* transcribed with biotin-labelling mix (Roche, 75501920) and annealed with unlabeled reverse strands. The dsRNAs and protein were mixed in 1 x binding buffer (10 x storage: 80% glycerol, 100 mM $MgCl_2$, 5 M NaCl, 0.5 M EDTA, 1 M DTT, 1 M Tris-HCl, pH 8.0), followed by incubation at room temperature for 15 minutes. Subsequently, the protein-RNA mixture was electrophoresed using a 6% native-PAGE gel at 80 V for 2 hours in 1x running buffer (25 mM Tris, 0.5 M glycine) and then transferred onto a nylon membrane using a transfer apparatus and 0.5 x TBE buffer for 4 hours. UV cross-linking was performed at a dose of 0.12 J/cm² using a 254 nm UV source for 50 seconds to immobilize the complex on the nylon membrane. Finally, biotin-labeled RNAs were detected using stabilized streptavidin-HRP.

RNA-IP

Dyna Protein G beads (25 μL) were added to each sample in an RNase-free microcentrifuge tube, which was placed on a magnetic stand for 30 seconds. After careful removal of the supernatant, the beads were washed twice with 1 mL of IP-blocking buffer (0.5% BSA in PBS) and incubated with 25 μL of IP-blocking buffer and 3 μL anti-His antibody overnight at 4 ^{o}C with rotation to facilitate antibody binding. The antibody-coated beads were then washed thrice with the IP-blocking buffer.

In parallel, the Prkra-His protein and biotin-labeled dsRNAs were incubated in a protein-RNA binding buffer at room temperature for 20 minutes in a 50 μL reaction volume. After adding 500 μL of 1 x binding buffer and 25 μL of prepared anti-His beads, the mixture was incubated at room temperature under rotation for 30 minutes. Subsequently, the magnetic beads were gently washed thrice with 1 x binding buffer, followed by adding TE buffer. The grasped biotin-labeled RNAs were released by boiling at 95 ^{o}C for 5 minutes. Dot blot analysis was performed using the stabilized streptavidin-HRP conjugate to visualize Prkra interacting RNAs.

SVCV preparation and injection

Spring viremia of carp virus (SVCV) viral suspension stored at -80 °C was thawed on ice. EPC cells with a density of 80%-90% in serum-free M199 medium (Hyclone) were rinsed in cell culture flasks. The

viral suspension was inoculated into the cells at a 1% volume ratio. The infection was carried out at 25 °C for 2 hours with intermittent shaking for 3-5 times. After viral infection, the viral fluid was collected, and the cell maintenance medium containing 2% FBS (Gibco) in M199 cell culture medium was added to the flasks for further cultivation. EPC cell infection was examined using an inverted microscope at 48-96 hours of cultivation. When more than 80% of cells exhibited cytopathic effects (CPEs), the flasks were subjected to three cycles of freeze-thawing in a -80 °C freezer, followed by centrifugation at 4 °C, 845 g for 10 minutes. The collected supernatant was aliquoted into 2 mL cryovials and stored at -80 °C for future use. EPC cells were seeded in a 96-well cell culture plate at a density of 1 x 10^4 cells per well and cultured at 25 °C for 16-24 hours. When cell confluence reached 80%-90%, 100 μL of virus suspension at dilutions ranging from 10^{-1} to 10^{-10} was added to each well, with four replicates per dilution and three parallel experimental groups. The CPEs of monolayer cells at each dilution were examined every 24 hours. The semi-logarithmic Reed-Muench method was employed to calculate the half-tissue culture infectious dose ($TCID_{50}$) of SVCV (30). Zebrafish embryos were injected with 2 nL of SVCV at a 5 x 10^6 $TCID_{50}$/mL concentration. Embryos were collected at 2-hour intervals, and the total viral load was quantified using qRT-PCR (primers in Supplementary Table S2). Subsequently, a viral growth curve was generated based on the levels of SVCV replication.

Quantification and Statistical Analysis

All experiments were repeated at least two times with similar results. Data plotting and statistical tests were performed using GraphPad Prism 9. Statistical information is described in the figure legends.

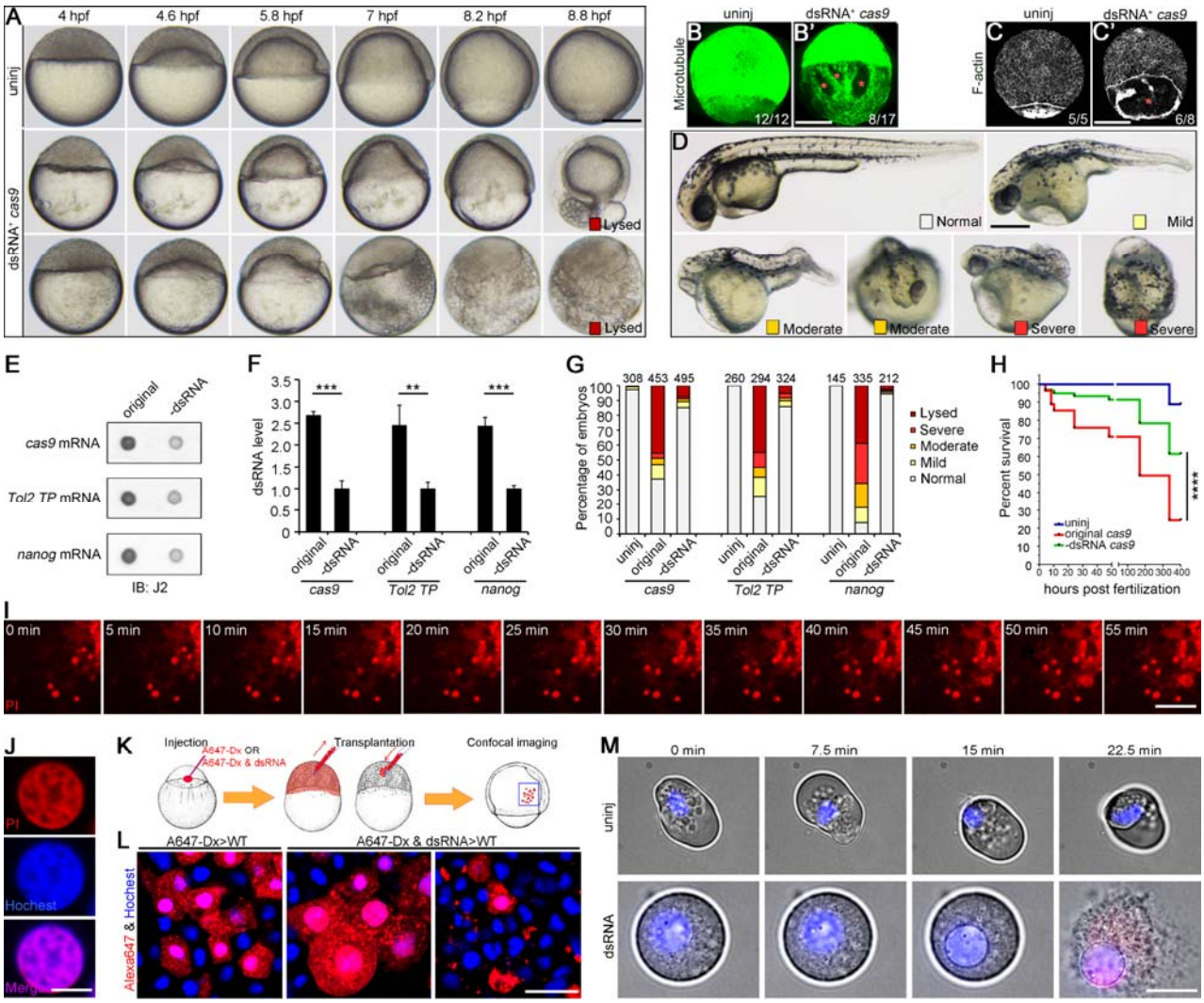

Figure 1. Injection of dsRNAs induces malformation and cell necrosis in zebrafish embryos. (**A**) Lysed phenotypes in gastrula stage embryos previously injected with *cas9* mRNAs. (**B-C'**) Cytoskeleton defects in IVT mRNA-injected embryos, with asterisks indicating cytoskeleton-free regions in the yolk cortical layer. (**D**) Toxic phenotypes at 36 hpf. (**E** and **F**) Reduction of dsRNA by-products after cellulose chromatography. (**G** and **H**) Decreased occurrence of malformed embryos and significantly increased survival rate upon dsRNA removal. (**I-J**) Appearance of PI-stained red nuclei in dsRNA-injected embryos. (**K** and **L**) Transplantation of labeled cells shows swelling and rupture morphology caused by dsRNA stimulation. (**M**) Live imaging captures the process of cell necrosis in dsRNA-injected cells. Values are means ± SDs. ** $p<0.01$, *** $p<0.001$, **** $p<0.0001$, Student's t-test in **F** and Gehan-Breslow-Wilcoxon test in **H**. Scale bars: 200 μm for **A-D**; 100 μm for **I**; 10 μm for **J**; 50 μm for **L**; 20 μm for **M**.

Results

Cell necrosis induced by dsRNAs present in IVT mRNAs

In vitro transcription often generates dsRNA by-products via 3'-end extension and antisense strand transcription (31-33). Accordantly, injection of IVT mRNAs into zebrafish embryos frequently causes toxicity, as indicated by massive deaths and malformed embryos, which are analogous to the malformations induced by dsRNAs (34). Although early cleavage was not affected (Video S1), *cas9* mRNA-injected embryos (200 pg/embryo) exhibited general developmental delay beginning at the onset of epiboly movement (Figure 1A and Video S2). More than one-fifth of injected embryos lysed during the gastrula

stage, probably due to disrupted cortical F-actin and microtubule cytoskeletons in the cortical layer of the yolk cell (Figures 1B, 1B', 1C and 1C'). Injected embryos that survived at 36 hours postfertilization (hpf) exhibited developmental defects, such as tail truncation, split axis, abnormality or absence of eyes, malformed brain structures, and cardiac edema (Figure 1D).

Next, we used cellulose chromatography to reduce dsRNA by-products in IVT mRNAs (35), resulting in a 60%-80% decrease in dsRNA levels (Figures 1E and 1F). As expected, injection of purified mRNAs (200 pg/embryo) significantly reduced toxic effects (Figure 1G). The removal of dsRNA also led to a well-improved survival rate (Figure 1H). Moreover, injection of dsRNAs (100 pg/embryo) with different lengths (285 bp-1043 bp) and sequences (Supplementary Figure S1A and Supplementary Table S1) induced similar lethal phenotypes as observed after injection of IVT mRNAs (Supplementary Figure S1B-S1D). These results suggest that dsRNA, as a molecular pattern, is sufficient and necessary to cause toxic effects in the early embryo in a sequence-independent manner. We thus mainly used a 1 kb dsRNA from the 5' region of the *cas9* mRNA sequence in the following experiments.

To probe into the cellular basis of dsRNA-induced toxicity, we stained dsRNA-injected live embryos with propidium iodide (PI). Red fluorescent nuclei gradually emerged during development (Figures 1, I and J, Video S3), indicating a loss of membrane integrity. In cell transplantation and sectioning experiments, large swollen and broken cells were frequently observed in gastrula embryos, reminiscent of necrosis (Figures 1K, 1L, S1E and S1F). The process of cell membrane rupture was also captured in isolated single cells (Figure 1M and Video S4). Consistent with frequent membrane rupture, F-actin lining the cell membrane was remarkably reduced in swollen cells after dsRNA injection (Supplementary Figure S1G and S1H). By transmission electron microscopy (TEM), we also observed active mitophagy occurring in swollen cells induced by dsRNAs (Supplementary Figure S1I-S1N), suggesting a potential self-rescue response to mitigate the dsRNA-stimulated stress. These data demonstrate that dsRNAs cause toxicity by inducing cell necrosis in the early embryo.

The dsRNAs induce an ISR-like translation blockage independently of PKR and phospho-eIF2α

There is a possibility that the toxic effects arise due to a widespread translation blockage by dsRNA-induced ISR. To verify this hypothesis, we injected *gfp* reporter mRNAs along with annealed dsRNAs or dsRNA-containing *cas9* IVT mRNAs. Compared with injection of *gfp* mRNAs alone (150 pg/embryo), coinjection of dsRNAs (30 pg/embryo) with *gfp* mRNAs remarkably reduced GFP protein levels by over 90%, and coinjection of dsRNA-positive *cas9* mRNAs (100 pg/embryo) with *gfp* mRNAs also significantly reduced GFP protein synthesis, albeit to a lesser extent (Figures 2A and 2B). We also tested luciferase reporter mRNAs (150 pg/embryo) in the coinjection experiment and obtained similar results (Figure 2C). Therefore, there must be a translation blockage because the integrity and expression levels of *gfp* mRNA were unaffected after dsRNA coinjection (Figure 2D). Next, we performed puromycin incorporation experiments to determine if global translation inhibition occurs upon dsRNA stimulation. Similar to the positive control in which cycloheximide (CHX) treatment was used to block translation, we observed a dramatic decrease in puromycin-labeled protein levels after injecting dsRNA-containing IVT mRNAs (200 pg/embryo) or annealed dsRNAs (100 pg/embryo) (Figures 2E-2G). By analyzing the ribosome profile through sucrose density gradient ultracentrifugation, it was evident that dsRNA stimulation significantly reduced the levels of polysomes (Figures 2H and 2I).

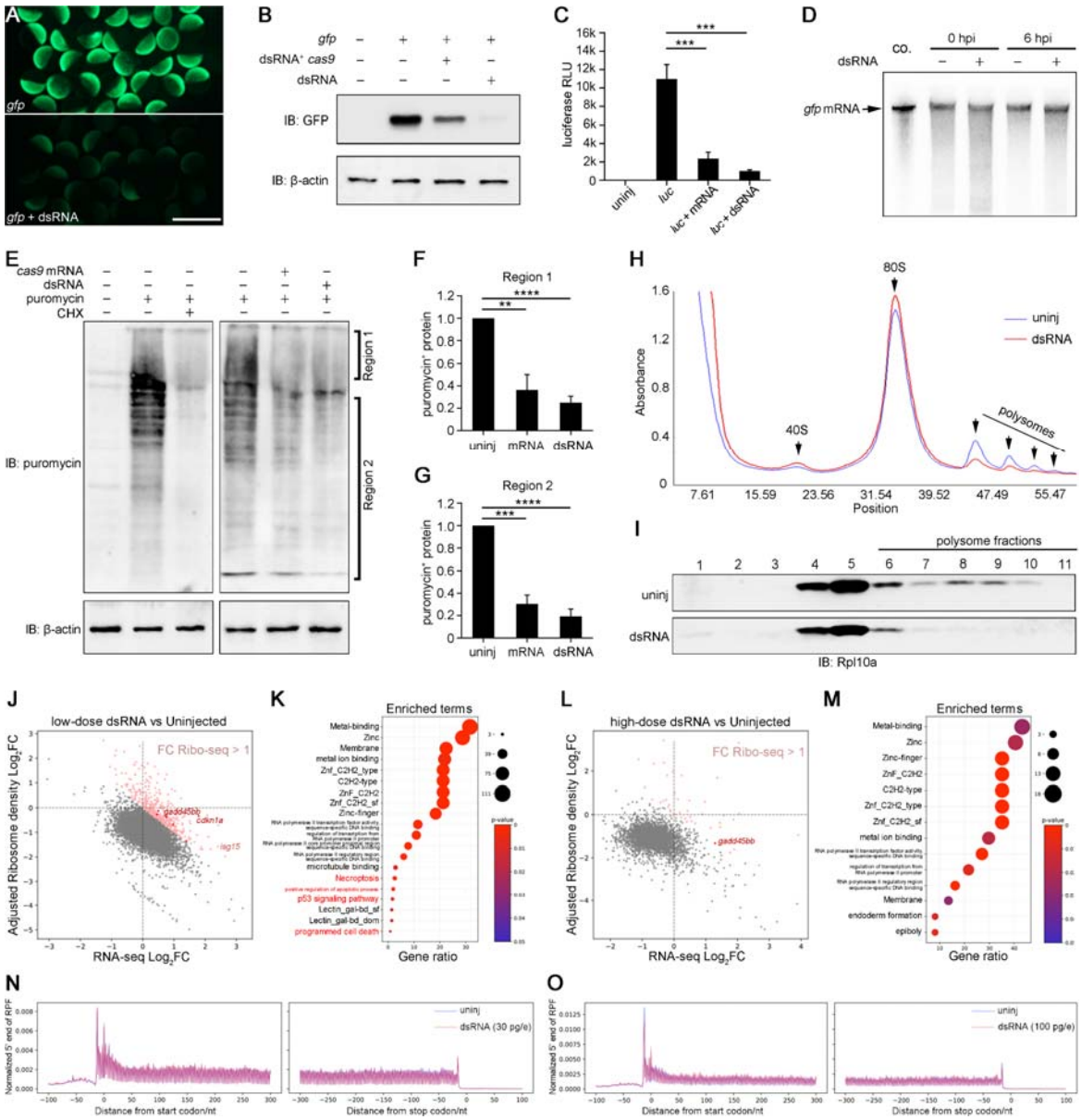

Figure 2. dsRNAs induce an ISR-like global translation repression. (**A**) Significant suppression of GFP expression in embryos injected with dsRNAs (30 pg/embryo), as revealed by fluorescent imaging. (**B**) Representative western blot results and quantification. (**C**) dsRNAs suppress luciferase activity produced by *luciferase* reporter mRNA. (**D**) Northern blot analysis shows the absence of degradation of *gfp* and *luciferase* reporter mRNAs by dsRNAs. (**E**) Reduced puromycin incorporation shows significantly reduced newly synthesized proteins after injection of dsRNAs in zebrafish embryos. (**F-G**) Quantification of regions 1 and 2. (**H**) Ribosome profile comparison between uninjected and dsRNA-injected embryos at 6 hpf. (**I**) Western blot analysis of Rpl10a in fractions separated by sucrose gradient ultracentrifugation. (**J** and **L**) Changes in mRNA abundance and translation efficiency (adjusted ribosome density) after stimulation with low dose (**J**) and high dose (**L**) dsRNAs. Pink-red designates genes with enhanced protein synthesis rates. Dark red indicates p53 target genes. (**K** and **M**) Enriched terms of genes with upregulated protein synthesis. Red highlights cell death-related terms. (**N** and **O**) 5' end distribution of ribosome footprints on mRNAs from uninjected and dsRNA-injected embryos. Values are means ± SDs. ** p<0.01, *** p<0.001, **** p<0.0001, Student's *t*-test. Scale bar: 1 mm

To further characterize the dsRNA-induced global translation blockage, we performed ribosome profiling (Ribo-seq) analysis on dsRNA-injected embryos (28), after injection of either low dose (30 pg/embryo) or high dose (100 pg/embryo) of dsRNAs. Ribo-seq has collectively generated 16.07 M uniquely mapped reads. The high quality of Ribo-seq data was confirmed by the length of ribosome-protected fragments (RPFs), the triplet periodicity of 5' ends mapping of RPFs, and the pairwise correlation of two replicates (Supplementary Figure S2A-S2E). After incorporating correction factors according to puromycin incorporation (Supplementary Figure S2F and Materials and Methods), over 97.2% of transcripts showed down-regulated translation efficiency upon dsRNA injection (Figures 2J and 2L, Data S1 and Materials and Methods). Protein production after dsRNA stimulation was also examined by assaying the adjusted RPF counts of each gene. In embryos injected with low dose of dsRNAs, the protein synthesis rate of 389 genes representing 4.41% of tested genes remained unaffected or even enhanced (Figure 2J and Data S1). GO analysis highlighted terms related to zinc finger and sequence-specific DNA binding. This analysis also enriched the p53 pathway and other cell death-related terms (Figure 2K). However, in embryos injected with high dose of dsRNAs, only 43 genes, representing 1.25% of tested genes, showed a high rate of protein synthesis (Figure 2L and Data S1). GO analysis revealed a similar enrichment of zinc finger-related transcription factors (Figure 2M). These findings demonstrate an ISR-like translatomic reshaping after dsRNA injection into the early embryos.

Next, we analyzed the distribution of 5' ends of RPFs. Surprisingly, in the background of the robust global translation blockage, dsRNA stimulation did not alter the normalized occupancy of ribosomes either at the 5' regions of open reading frames (ORFs) or the positions near the stop codon (Figures 2N and 2O). As Ribo-seq only captures the translation process after loading the 43S preinitiation complex onto mRNAs, the similar distribution of RPFs suggests that dsRNAs primarily affect the early phase of translation initiation, occurring before the loading of ribosomes. However, ribosome scanning and translation elongation appear to proceed normally.

Does the PKR-eIF2α axis mediate the ISR-like translational repression? Intriguingly, *eif2ak2* was expressed in trace amounts in the early embryo (Data S2) (17). Only extremely high doses of dsRNAs (300 pg/embryo) could induce eIF2α phosphorylation (Supplementary Figure S3A and S3B), suggesting that PKR/eIF2α axis is unlikely to be responsible for dsRNA-induced translation inhibition in the early zebrafish embryo. To definitively rule out this possibility, we generated a maternal-zygotic (MZ) mutant for *eif2ak2* (MZ*eif2ak2*) through the "CRISPant" approach (Supplementary Figure S3C) (18). In contrast to the wild-type (WT) embryos, MZ*eif2ak2* mutants injected with dsRNAs (300 pg/embryo) failed to phosphorylate eIF2α (Supplementary Figure S3D). However, the translation was still vigorously blocked, comparable to wild-type embryos (Supplementary Figure S3E). These results collectively indicate that dsRNAs induce ISR-like phenomena in the early embryo by a distinct dsRNA sensor that functions independently of the PKR-eIF2α axis.

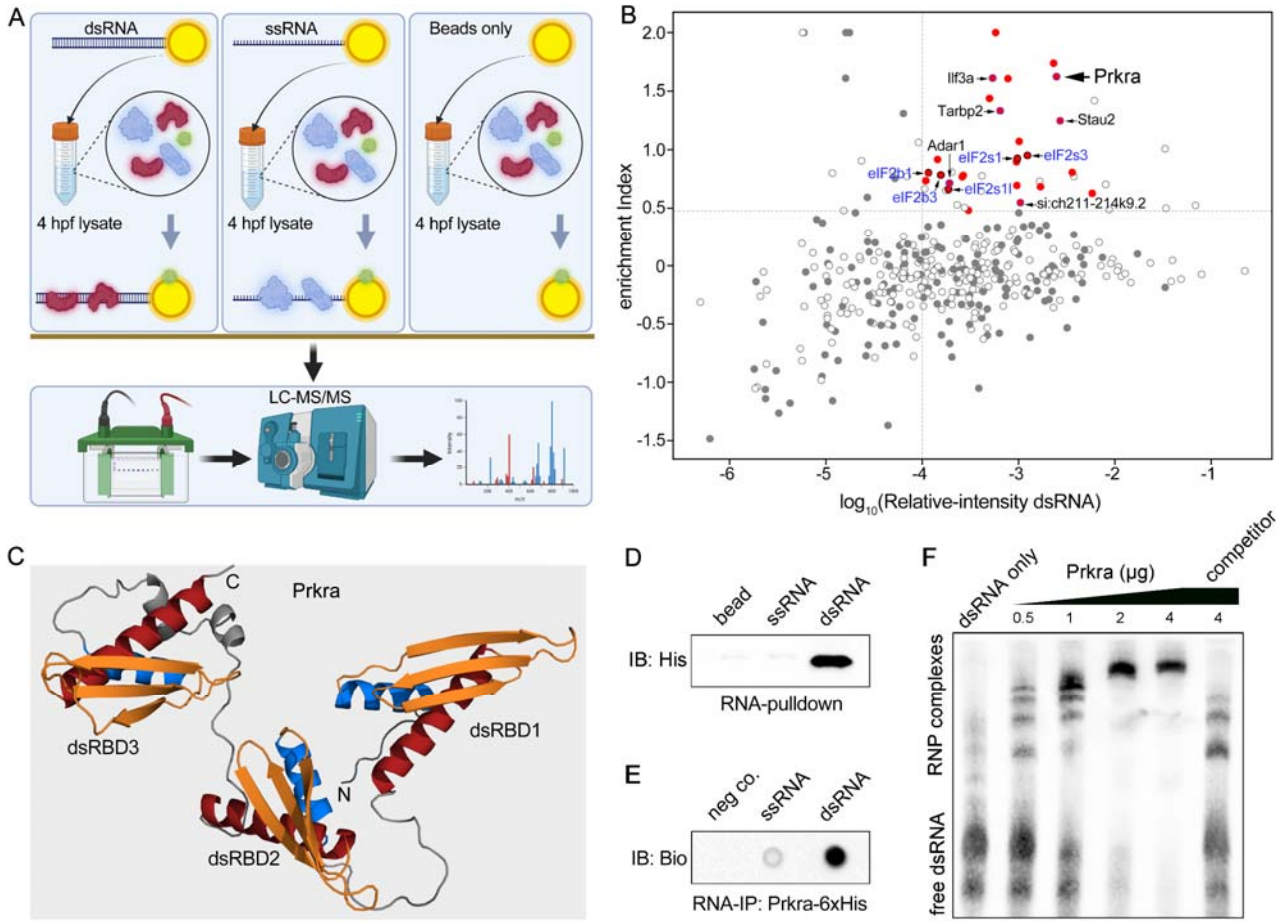

Figure 3. Prkra recognizes dsRNAs in the early embryo. (**A**) Experimental design of RNA-pulldown followed by MS. (**B**) Scatter plot showing enrichment with respect to relative intensity. Specific dsRNA-associated components are highlighted by red dots (see Materials and Methods and Data S3). Known dsRBPs are in black; eIF2 and eIF2B components are in blue. Grey circles represent proteins with high contamination in RNA-free beads. (**C**) Predicted putative structure of Prkra by Alphafold2, highlighting the three dsRBDs with the short α-helix designated in blue, three β-sheets in orange and the long α-helix in dark red. (**D**) RNA pulldown shows the specific interaction of His-tagged Prkra with dsRNAs. (**E**) RNA IP shows the specific binding of biotin-labeled dsRNAs by His-tagged Prkra. (**F**) EMSA analysis shows the dsRNA-binding capacity of His-tagged Prkra.

Prkra is the dsRNA sensor mediating translation blockage in the early embryo

We performed stringent RNA-pulldown experiments using biotinylated dsRNAs as bait to identify the genuine dsRNA sensor responsible for translation control. Single-stranded RNAs (ssRNAs) and RNA-free beads were used as negative controls (Figure 3A). By analyzing the abundance and specificity of proteins pulled down by dsRNAs (see Methods), we identified a total of 26 proteins (Figure 3B and Data S3), including six known dsRNA-binding proteins (dsRBPs) and five subunits of the eIF2 and eIF2B complexes. In particular, GO analysis highlighted “dsRNA binding”, “translation initiation”, “eIF2 complex” and “eIF2B complex” in the enriched terms (Supplementary Figure S4).

Among the candidate dsRBPs, Prkra is a promising candidate for a dsRNA sensor because it exhibited a remarkable enrichment of over 70 folds in the pulldown experiments using dsRNAs compared to ssRNAs and achieved one of the highest intensities (Figure 3B and Data S3). Notably, the zebrafish Prkra protein consists of 282 amino acid residues and adopts a folded structure comprising three tandem dsRNA-binding domains (dsRBDs). Each dsRBD is characterized by a short α helix, three β-folds, and a lengthy α helix shared by most dsRBPs (Figure 3C) (36). We then conducted biochemical analyses to validate its dsRNA-

binding capacity and specificity. Consistent with the mass spectrometry (MS) data, recombinant Prkra from *E. coli* binds explicitly to dsRNAs but not ssRNAs (Figures 3D and 3E). The electrophoretic mobility shift assay (EMSA) experiments unequivocally demonstrated the robust binding capacity of Prkra to dsRNAs (Figure 3F). The molecular weight of the Prkra-dsRNA complexes was significantly increased with the addition of more proteins, indicating the formation of dsRNA-associated Prkra polymers (Figure 3F). Unlabeled dsRNAs were able to compete with biotinylated dsRNAs for binding to Prkra, as evidenced by the decreased molecular weight of the Prkra-dsRNA complex (Figure 3F), further demonstrating the specific interaction between Prkra and dsRNAs. These data thus indicate that Prkra may function as a dsRNA sensor in the early embryo.

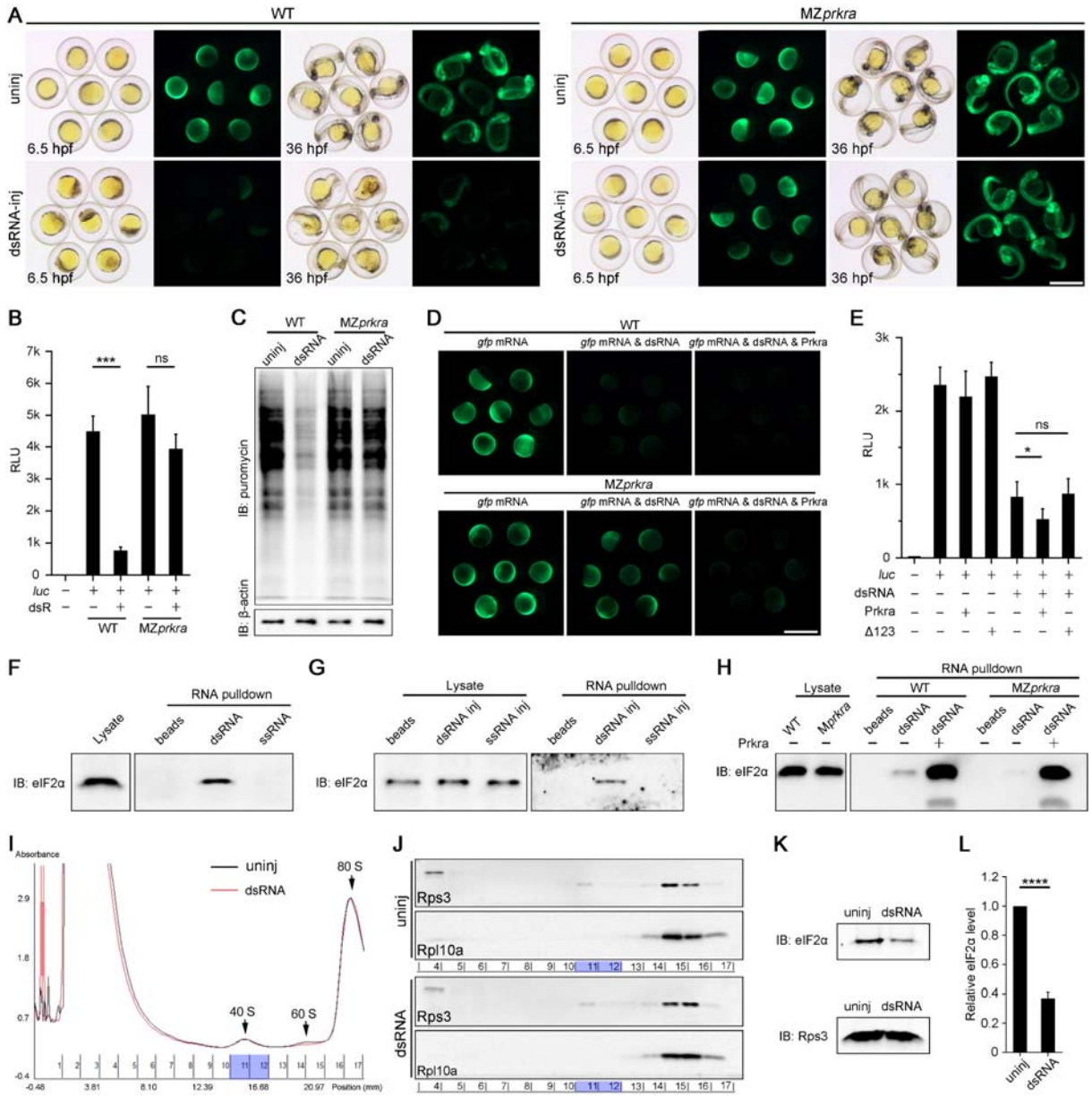

Figure 4. Prkra is a dsRNA sensor for translational repression by depletion of the eIF2 complex. (**A**) Comparison of *gfp* IVT mRNA translation in WT embryos and MZ*prkra* mutants in response to dsRNA stimulation. (**B**) Analysis of *luciferase* mRNA translation in WT embryos and MZ*prkra* mutants in the presence of dsRNAs. (**C**) Puromycin incorporation showing decreased global protein synthesis upon dsRNA stimulation. (**D**) Prkra enhances translation blockage by dsRNAs in both WT embryos and MZ*prkra* mutants. (**E**) Translation blockage by dsRNAs in the rabbit reticulocyte *in vitro* translation system

is enhanced by recombinant Prkra but not mutant Prkra (with the lengthy α-helix in each dsRBD deleted: Δ123). (**F**) Pulldown experiment shows bead-immobilized dsRNAs specifically interact with eIF2α in 4-hpf embryo lysates. (**G**) Biotinylated dsRNAs injected into the embryos specifically interact with eIF2α. (**H**) Recombinant Prkra strongly enhances the interaction between dsRNAs and eIF2α. (**I** and **J**) Analysis of the amount of 43S preinitiation complex by fragments isolated from sucrose gradient ultracentrifugation. (**K** and **L**) Significant decrease in 43S preinitiation complex in the presence of dsRNAs. Values shown are means ± SDs. * $p<0.05$, *** $p<0.001$,**** $p<0.0001$, ns $p>0.05$, Student's *t*-test. Scale bars: 1 mm for **A** and **D**.

For functional validation, we next generated MZ*prkra* mutants using the CRISPR/Cas9 approach. Disruption of the *prkra* gene resulted in nonsense-mediated decay occurring in all F1 early embryos, as demonstrated by the results of in situ hybridization (ISH) and RT-PCR (Supplementary Figure S5A and S5B), indicating complete removal of *prkra* gene products. Injection of 50 pg dsRNAs into the MZ*prkra* embryo resulted in very mild or no phenotypes, with most embryos developing normally. In contrast, an equal amount of dsRNAs in wild-type embryos induced lethal malformations (Supplementary Figure S5C and S5D). Consistent with the remarkably weakened phenotypes, *prkra* mutation significantly alleviated the translational inhibition of IVT *gfp* and *luciferase* mRNAs mediated by dsRNAs (Figures 4A and 4B). The dsRNA-mediated blockage of puromycin incorporation was also released in MZ*prkra* mutant embryos (Figure 4C). Conversely, coinjection of Prkra protein into wild-type embryos enhanced translation inhibition, while coinjection into MZ*prkra* embryos also potentiated dsRNA-mediated translation suppression (Figure 4D). Significantly, in a reticulocyte lysate *in vitro* translation system, the addition of dsRNAs led to a decreased translation, and the presence of wild-type but not mutant Prkra (with the lengthy α-helix in each dsRBD deleted) further enhanced the translational repression (Figure 4E).

Prkra-dsRNA hijacks the eIF2 complex to inhibit the formation of the 43S preinitiation complex

The RNA pulldown and MS data revealed the specific interaction of dsRNAs with eIF2 and eIF2B complexes (Figures 3B and S4). Thus, the dsRNA-Prkra complex might grasp the eIF2 complex, pulling it away from the translation machinery. To test this hypothesis, we first confirmed the specific interaction between dsRNAs and eIF2α *in vitro* and *in vivo* through RNA-pulldown and western blot analyses (Figures 4F and 4G). Importantly, this interaction was dependent on the presence of Prkra, as evidenced by the significantly reduced binding of eIF2α to dsRNAs when using lysates from MZ*prkra* embryos (Figure 4H). Conversely, the addition of recombinant Prkra to the lysates derived from either wild-type or MZ*prkra* embryos resulted in a remarkable increase in the amount of pulled-down eIF2α (Figure 4H).

Considering that eIF2 subunits play a crucial role in the assembly of the 43S preinitiation complex to regulate the rate of translation initiation, it is crucial to determine whether binding of eIF2 to the Prkra-dsRNA complex is sufficient to reduce the formation of the 43S preinitiation complex. To address this question, we conducted fragmentation experiments using sucrose density gradient ultracentrifugation. Fragments located near the 40S ribosome region were isolated based on the A260 profile (Figure 4I) and western blot analyses using small and large ribosome markers (Figure 4J). Notably, the amount of eIF2α, serving here as a marker for the 43S preinitiation complex, exhibited a significant decrease (Figures 4K and L), which corresponded to the observed reduction in global protein synthesis levels. These results thus identified a Prkra-dependent eIF2 complex sequestering mechanism to cause global translation blockage.

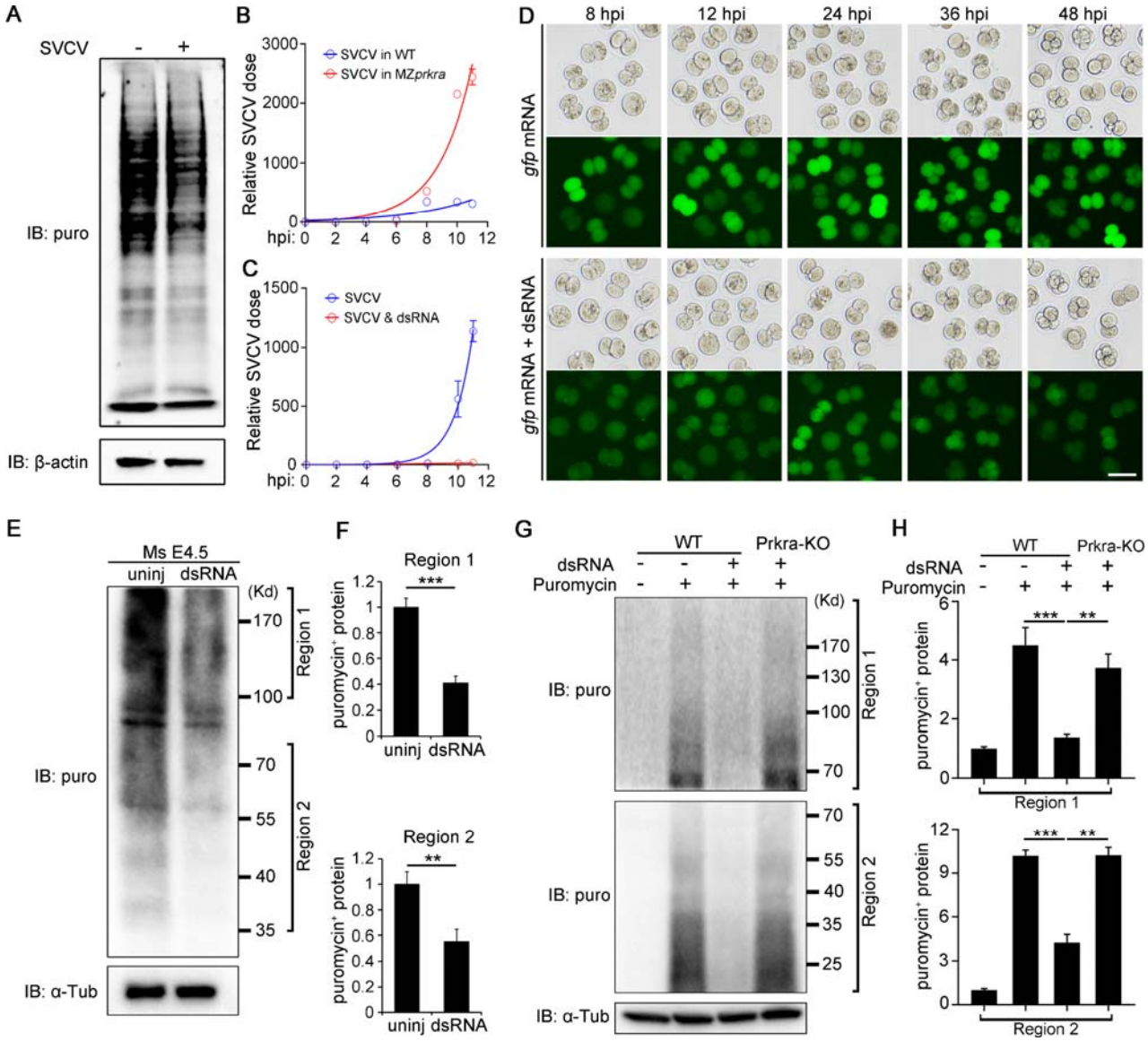

Figure 5. Antiviral activity of Prkra and conservation of embryonic ISR. (**A**) Global reduction of protein synthesis induced by SVCV in the early embryo. (**B**) Enhanced replication of SVCV in MZ*prkra* mutant embryos. hpi: hours post-injection. (**C**) Suppression of SVCV replication by coinjecting dsRNAs. (**D**) dsRNAs significantly reduce the translation of *gfp* mRNAs in early mouse embryos. hpi: hours post-injection.

(**E**) Inhibition of puromycin incorporation in newly synthesized proteins by dsRNA stimulation. (**F**) Quantification of puromycin-positive proteins in regions 1 and 2. (**G** and **H**) Robust translation inhibition by dsRNA in WT mESCs but not in *Prkra* mutants. Values shown are means ± SDs. * $p<0.05$, ** $p<0.01$, *** $p<0.001$, **** $p<0.0001$, ns $p>0.05$, Student's *t*-test. The data in **B** and **C** are least-squires fitted according to the logistic growth curve. Scale bar: 100 μm.

Embryonic ISR restricts virus replication

To determine whether the dsRNA-induced response represents a valid antiviral mechanism in the early embryo, spring viremia of carp virus (SVCV), a negative-sense RNA virus, was introduced into zebrafish embryos. Six hours after injection of the virus, we found a significant inhibition of translation, as demonstrated by the puromycin incorporation assay, which showed an approximately 50% overall reduction of protein levels (Figure 5A). To examine whether this Prkra-dependent ISR can inhibit viral replication, we injected SVCV into MZ*prkra* embryos. Compared to WT embryos, the SVCV exhibited an

explosive replication trend in MZ*prkra* mutants (Figure 5B). Notably, injecting dsRNAs to activate the embryonic ISR intentionally resulted in a nearly complete block of SVCV replication (Figure 5C). These results demonstrate that the translation blockage triggered by the dsRNA sensor Prkra is a fully functional antiviral innate immune response.

Conserved embryonic ISR in mice

Finally, we asked the question of whether the dsRNA-induced embryonic ISR represents a species-specific or a conserved event. This question was addressed by injecting *gfp* reporter mRNA into early mouse embryos with or without dsRNAs. As expected, injecting dsRNAs (100 pg/embryo) significantly suppressed overall GFP expression (Figure 5D). We also observed a 40%-60% reduction of newly synthesized proteins at around E4.5 in response to dsRNA stimulation (Figures 5E and 5F). The conservation of embryonic innate immune was also confirmed in mouse ESCs (mESCs). To analyze the role of mouse Prkra in innate immunity, we generated a *Prkra* knockout (*Prkra*-KO) mESC line (Supplementary Figure S6A). Western blot and qRT-PCR results showed an absence of Prkra protein and a significantly reduced transcript level in the mutant cell line (Supplementary Figure S6B and S6C). Importantly, the knockout of *Prkra* in mESCs almost abolished the translational inhibitory effect of dsRNAs (Figures 5G and 5H). These results demonstrate that Prkra is a conserved dsRNA sensor for translation control in early mammalian embryos and stem cells. They also suggest that the dsRNA-induced ISR in the early embryos represents a conserved process across species.

Discussion

This study characterized a unique ISR in vertebrate early embryos and stem cells. Prkra senses dsRNAs to trigger a global translation inhibition, which leads to profound developmental malformation and cell necrosis. These effects are quite different from the canonical ISR, because the global translation blockage following dsRNA stimulation is independent of PKR and the eIF2α phosphorylation but is mediated by a Prkra-dependent depletion of the eIF2 complex from the translation machinery.

This unique embryonic ISR may represent a primordial antiviral strategy that has evolved over millions of years. Prkra homologs are widely distributed across diverse taxa, including invertebrates such as crustaceans and sponges. Intriguingly, similar proteins are also present in plants, exemplified by the unnamed protein product CAD5324251.1 in *Arabidopsis thaliana*. This broad phylogenetic distribution strongly suggests an ancient evolutionary origin predating the divergence of plants and animals. In contrast, the PKR-induced ISR appears to be a more recent evolutionary innovation confined to vertebrates. Two key observations support this hypothesis: First, the IFN system, a critical component of antiviral immunity, is found exclusively in vertebrates (37). Second, PKR is a well-characterized ISG that functions downstream of the IFN signaling.

Why do early embryos and undifferentiated cells require mechanisms independent of PKR and phospho-eIF2 to combat viruses? One possible explanation is that PKR expression requires the activation of IFN signaling. However, the activation of IFN can inhibit proliferation and promote stem cell differentiation by upregulating a full spectrum of ISGs (16,38-40). This may be particularly detrimental to maintaining pluripotency/multipotency of stem cells and the normal development of early embryos. Another possibility is that the early embryo may employ a cell-autonomous antiviral strategy that confers advantages by restricting stress responses to a small portion of the population. The pronounced translation blockage, cell necrosis and eventual individual death triggered by the embryonic ISR could be perceived as altruistic behavior, as these processes further limit the release of viruses in membrane-coated infectious forms. Further investigations into the molecular mechanisms underlying these antiviral strategies will provide valuable insights into the delicate balance between host defense and developmental processes during early embryogenesis.

The robust stress response induced by dsRNA interprets the challenges of employing siRNA-mediated knockdown in animal models like zebrafish, Xenopus, and others (41,42). Mouse embryos, however, may exhibit lower sensitivity to dsRNA-induced embryonic ISR or higher RNAi efficiency than zebrafish, making siRNA-mediated knockdown still feasible in this context. Nevertheless, avoiding excessive siRNA injection in early mouse embryos should be crucial to prevent unspecific toxic effects conferred by

activating embryonic ISR. Our study also highlights the potential risks associated with the indiscriminate use of synthetic mRNAs for gene functional studies and therapeutics in undifferentiated cells. Activation of the embryonic ISR by dsRNA by-products can lead to non-specific toxic phenotypes, which may compromise the specificity and accuracy of mRNA-mediated gene overexpression. Therefore, it is crucial to carefully evaluate the global translation levels following the introduction of mRNA to prevent unintended consequences and ensure the reliability of experimental and therapeutic outcomes.

In conclusion, our study reveals a dsRNA sensor analogous to PKR that is crucial in regulating ISR-like translation inhibition in pluripotent cells. Future investigations should aim to elucidate the extent to which this embryonic ISR compensates for the canonical ISR in differentiated cells. Additionally, evaluating the potential of the embryonic ISR to contribute to the development of novel antiviral and anti-tumor treatments would be of great interest.

Data availability

The deep sequencing data of Ribo-seq are available from NCBI Gene Expression Omnibus GSE234230. The scripts are available at https://github.com/benjaminfang/ribo-seq-workflow. Further information and requests for resources and reagents should be directed to and will be fulfilled by the corresponding author, Ming Shao (shaoming@sdu.edu.cn).

Supplementary Data statement

Document S1. Supplementary Figure S1-S6 and Tables S1-S2

Video S1. Live imaging of uninjected and *cas9* IVT mRNA-injected embryos, related to Figure 1.

Video S2. Live imaging of the gastrulation process of uninjected and *cas9* IVT mRNA-injected embryos, related to Figure 1.

Video S3. PI staining of live embryos injected with dsRNAs, related to Figure 1.

Video S4. Isolated dsRNA-stimulated cells undergoing necrosis, related to Figure 1.

Data S1. (separate file) Metadata spreadsheet of Ribo-seq data.

Data S2. (separate file) Expression of genes mentioned in this study.

Data S3. (separate file) Metadata spreadsheet of dsRNA pulldown followed by LC-MS/MS.

Data S4. (separate file) Raw data visualized in each Figure.

Data S5. (separate file) Uncropped blots presented in this paper.

Acknowledgements

We are grateful to professor Li Yu for sharing his ideas for improving the work. We thank J.L.S and H.J.D from the Core Facility and Service Platform, School of Life Sciences, H.Y.Y and X.M.Z from SKLMT for assistance with confocal imaging, histological sectioning and ribosome profiling, and Z.X.D for fish rearing.

Funding

This work was supported by National Natural Science Foundation of China 32370860, 32170816, 31871451 to M.S., 31771526 to X.G.L., Program of Outstanding Middle-aged and Young Scholars of Shandong University to M.S., Science and Technology Department of Yunnan Province (202305AH340007) to B.Y.M., and the Earmarked Fund for CARS (CARS-45) to Y.Z.

Conflict of Interest Disclosure

China patent 202310609693.3 has been authorized to MS, TL and AJC for the application of zebrafish embryos for dsRNA by-product detection.

References

1. Hur, S. (2019) Double-Stranded RNA Sensors and Modulators in Innate Immunity. *Annu Rev Immunol*, **37**, 349-375.
2. Carpenter, S. and O'Neill, L.A.J. (2024) From periphery to center stage: 50 years of advancements in innate immunity. *Cell*, **187**, 2030-2051.
3. de Reuver, R. and Maelfait, J. (2024) Novel insights into double-stranded RNA-mediated immunopathology. *Nat Rev Immunol*, **24**, 235-249.
4. Pain, V.M. (1996) Initiation of protein synthesis in eukaryotic cells. *Eur J Biochem*, **236**, 747-771.
5. Costa-Mattioli, M. and Walter, P. (2020) The integrated stress response: From mechanism to disease. *Science*, **368**.
6. Ryoo, H.D. (2024) The integrated stress response in metabolic adaptation. *J Biol Chem*, **300**, 107151.
7. Clemens, M.J. and Elia, A. (1997) The double-stranded RNA-dependent protein kinase PKR: structure and function. *J Interferon Cytokine Res*, **17**, 503-524.
8. Kenner, L.R., Anand, A.A., Nguyen, H.C., Myasnikov, A.G., Klose, C.J., McGeever, L.A., Tsai, J.C., Miller-Vedam, L.E., Walter, P. and Frost, A. (2019) eIF2B-catalyzed nucleotide exchange and phosphoregulation by the integrated stress response. *Science*, **364**, 491-495.
9. Wuerth, J.D., Habjan, M., Kainulainen, M., Berisha, B., Bertheloot, D., Superti-Furga, G., Pichlmair, A. and Weber, F. (2020) eIF2B as a Target for Viral Evasion of PKR-Mediated Translation Inhibition. *mBio*, **11**.
10. Jackson, R.J., Hellen, C.U. and Pestova, T.V. (2010) The mechanism of eukaryotic translation initiation and principles of its regulation. *Nat Rev Mol Cell Biol*, **11**, 113-127.
11. Jager, N., Pohlmann, S., Rodnina, M.V. and Ayyub, S.A. (2024) Interferon-Stimulated Genes that Target Retrovirus Translation. *Viruses*, **16**.
12. Gale, M., Jr., Tan, S.L. and Katze, M.G. (2000) Translational control of viral gene expression in eukaryotes. *Microbiol Mol Biol Rev*, **64**, 239-280.
13. Wuerth, J.D. and Weber, F. (2022) Shielding the mRNA-translation factor eIF2B from inhibitory p-eIF2 as a viral strategy to evade protein kinase R-mediated innate immunity. *Curr Opin Immunol*, **78**, 102251.
14. Burke, D.C., Graham, C.F. and Lehman, J.M. (1978) Appearance of interferon inducibility and sensitivity during differentiation of murine teratocarcinoma cells in vitro. *Cell*, **13**, 243-248.
15. Hong, X.X. and Carmichael, G.G. (2013) Innate immunity in pluripotent human cells: attenuated response to interferon-beta. *J Biol Chem*, **288**, 16196-16205.
16. Wu, X., Dao Thi, V.L., Huang, Y., Billerbeck, E., Saha, D., Hoffmann, H.H., Wang, Y., Silva, L.A.V., Sarbanes, S., Sun, T. *et al.* (2018) Intrinsic Immunity Shapes Viral Resistance of Stem Cells. *Cell*, **172**, 423-438 e425.
17. White, R.J., Collins, J.E., Sealy, I.M., Wali, N., Dooley, C.M., Digby, Z., Stemple, D.L., Murphy, D.N., Billis, K., Hourlier, T. *et al.* (2017) A high-resolution mRNA expression time course of embryonic development in zebrafish. *Elife*, **6**.
18. Moravec, C.E., Voit, G.C., Otterlee, J. and Pelegri, F. (2021) Identification of maternal-effect genes in zebrafish using maternal crispants. *Development*, **148**.
19. Moreno-Mateos, M.A., Vejnar, C.E., Beaudoin, J.D., Fernandez, J.P., Mis, E.K., Khokha, M.K. and Giraldez, A.J. (2015) CRISPRscan: designing highly efficient sgRNAs for CRISPR-Cas9 targeting in vivo. *Nat Methods*, **12**, 982-988.

20. Ying, Q.L., Wray, J., Nichols, J., Batlle-Morera, L., Doble, B., Woodgett, J., Cohen, P. and Smith, A. (2008) The ground state of embryonic stem cell self-renewal. *Nature*, **453**, 519-523.
21. Murakami, K., Terakado, Y., Saito, K., Jomen, Y., Takeda, H., Oshima, M. and Barker, N. (2021) A genome-scale CRISPR screen reveals factors regulating Wnt-dependent renewal of mouse gastric epithelial cells. *Proc Natl Acad Sci U S A*, **118**.
22. Xia, Y., Li, K., Li, J., Wang, T., Gu, L. and Xun, L. (2019) T5 exonuclease-dependent assembly offers a low-cost method for efficient cloning and site-directed mutagenesis. *Nucleic Acids Res*, **47**, e15.
23. Shao, M., Cheng, X.N., Liu, Y.Y., Li, J.T. and Shi, D.L. (2018) Transplantation of Zebrafish Cells by Conventional Pneumatic Microinjector. *Zebrafish*, **15**, 73-76.
24. Ingolia, N.T., Brar, G.A., Rouskin, S., McGeachy, A.M. and Weissman, J.S. (2012) The ribosome profiling strategy for monitoring translation in vivo by deep sequencing of ribosome-protected mRNA fragments. *Nat Protoc*, **7**, 1534-1550.
25. Langmead, B. and Salzberg, S.L. (2012) Fast gapped-read alignment with Bowtie 2. *Nat Methods*, **9**, 357-359.
26. Martin, M. (2011) Cutadapt removes adapter sequences from high-throughput sequencing reads. *EMBnet.journal*, **17**, 10-12.
27. Danecek, P., Bonfield, J.K., Liddle, J., Marshall, J., Ohan, V., Pollard, M.O., Whitwham, A., Keane, T., McCarthy, S.A., Davies, R.M. *et al.* (2021) Twelve years of SAMtools and BCFtools. *Gigascience*, **10**.
28. Ingolia, N.T., Ghaemmaghami, S., Newman, J.R.S. and Weissman, J.S. (2009) Genome-Wide Analysis in Vivo of Translation with Nucleotide Resolution Using Ribosome Profiling. *Science*, **324**, 218-223.
29. Sherman, B.T., Hao, M., Qiu, J., Jiao, X., Baseler, M.W., Lane, H.C., Imamichi, T. and Chang, W. (2022) DAVID: a web server for functional enrichment analysis and functional annotation of gene lists (2021 update). *Nucleic Acids Res*, **50**, W216-W221.
30. Zou, P.F. and Nie, P. (2017) Zebrafish as a Model for the Study of Host-Virus Interactions. *Methods Mol Biol*, **1656**, 57-78.
31. Triana-Alonso, F.J., Dabrowski, M., Wadzack, J. and Nierhaus, K.H. (1995) Self-coded 3'-extension of run-off transcripts produces aberrant products during in vitro transcription with T7 RNA polymerase. *J Biol Chem*, **270**, 6298-6307.
32. Gholamalipour, Y., Karunanayake Mudiyanselage, A. and Martin, C.T. (2018) 3' end additions by T7 RNA polymerase are RNA self-templated, distributive and diverse in character-RNA-Seq analyses. *Nucleic Acids Res*, **46**, 9253-9263.
33. Mu, X., Greenwald, E., Ahmad, S. and Hur, S. (2018) An origin of the immunogenicity of in vitro transcribed RNA. *Nucleic Acids Res*, **46**, 5239-5249.
34. Zhao, Z., Cao, Y., Li, M. and Meng, A. (2001) Double-stranded RNA injection produces nonspecific defects in zebrafish. *Dev Biol*, **229**, 215-223.
35. Baiersdorfer, M., Boros, G., Muramatsu, H., Mahiny, A., Vlatkovic, I., Sahin, U. and Kariko, K. (2019) A Facile Method for the Removal of dsRNA Contaminant from In Vitro-Transcribed mRNA. *Mol Ther Nucleic Acids*, **15**, 26-35.
36. Cottrell, K.A., Andrews, R.J. and Bass, B.L. (2024) The competitive landscape of the dsRNA world. *Mol Cell*, **84**, 107-119.
37. Iwama, R.E. and Moran, Y. (2023) Origins and diversification of animal innate immune responses against viral infections. *Nat Ecol Evol*, **7**, 182-193.
38. Hertzog, P.J., Hwang, S.Y. and Kola, I. (1994) Role of interferons in the regulation of cell proliferation, differentiation, and development. *Mol Reprod Dev*, **39**, 226-232.

39. Baldridge, M.T., King, K.Y., Boles, N.C., Weksberg, D.C. and Goodell, M.A. (2010) Quiescent haematopoietic stem cells are activated by IFN-gamma in response to chronic infection. *Nature*, **465**, 793-797.
40. de Veer, M.J., Holko, M., Frevel, M., Walker, E., Der, S., Paranjape, J.M., Silverman, R.H. and Williams, B.R. (2001) Functional classification of interferon-stimulated genes identified using microarrays. *J Leukoc Biol*, **69**, 912-920.
41. Tagami, Y., Nishiyama, T., Omote, M. and Watanabe, M. (2021) Application of the RNA interference technique to Xenopus embryos: Specific reduction of the beta-catenin gene products by short double-stranded RNA produced by recombinant human Dicer. *Development Growth & Differentiation*, **63**, 467-477.
42. Oates, A.C., Bruce, A.E. and Ho, R.K. (2000) Too much interference: injection of double-stranded RNA has nonspecific effects in the zebrafish embryo. *Dev Biol*, **224**, 20-28.

Supplemental information

Prkra is the double-stranded RNA sensor to mediate an embryonic integrated stress response

Tong Lu[1], Pengcheng Ma[2], Aijun Chen[1], Hailing Fang[1], Jianlin Xu[2], Mingyu Wang[3], Ling Su[1], Sen Wang[3], Yizhuang Zhang[1], Jiasheng Wang[1], Boya Yang[1], De-Li Shi[5], Yong Zhou[6], Qianqian Gong[1], Xiangguo Liu[1,7]*, Bingyu Mao[2,4]*, Ming Shao[1,7]*

Corresponding author: xgliu@sdu.edu.cn; mao@mail.kiz.ac.cn; shaoming@sdu.edu.cn

Supplemental information includes:

Supplementary Figures S1 to S6
Supplementary Tables S1 to S2

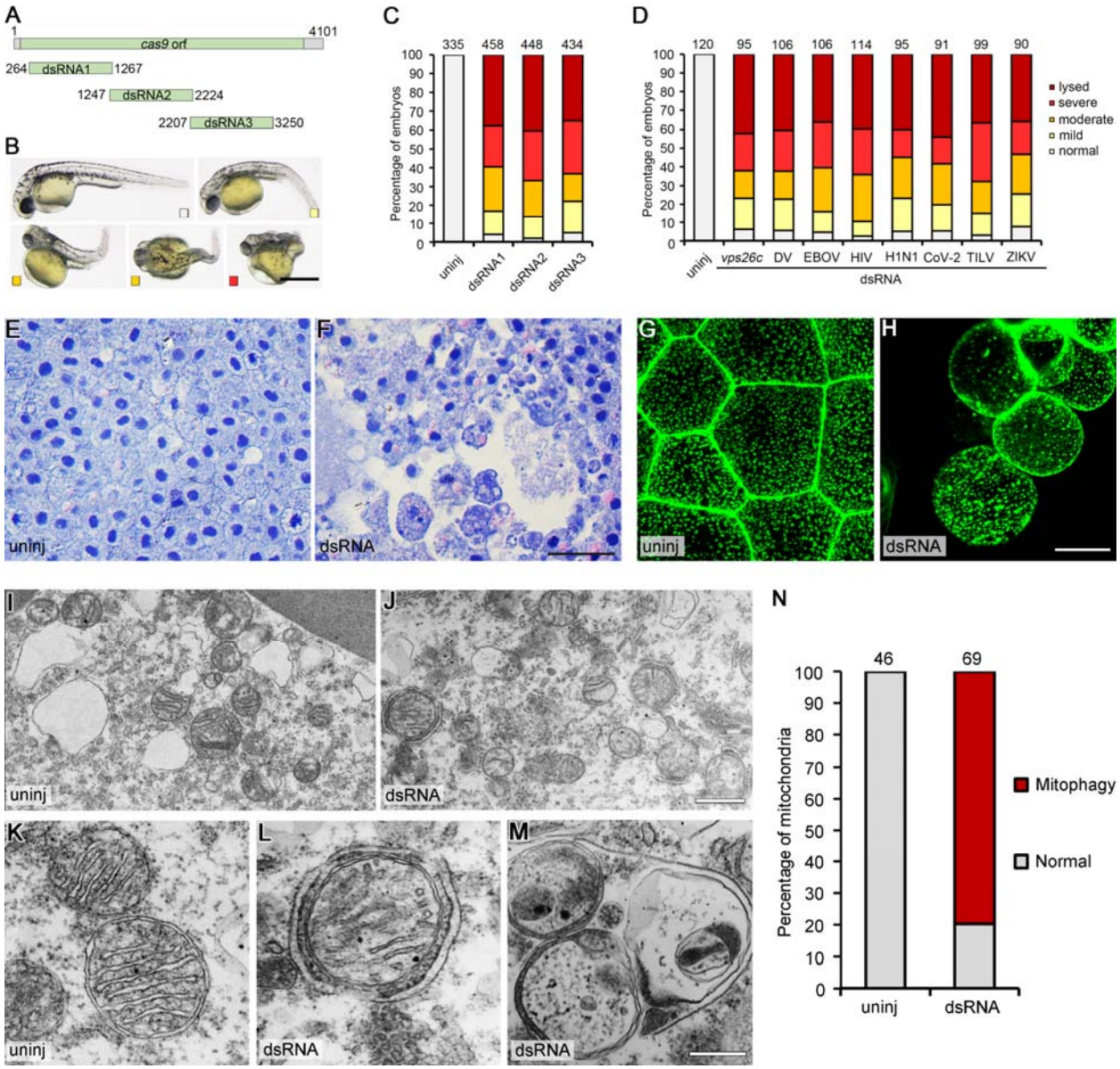

Supplementary Figure S1. dsRNAs cause necrosis and mitophagy, related to Figure 1. (**A**) dsRNAs derived from sequences of *cas9* mRNA. (**B**) Representative toxic phenotypes caused by dsRNA injection. (**C** and **D**) Phenotypic analysis caused by injection of dsRNAs from different sequence sources. (**E** and **F**) JB4 sections from uninjected and dsRNA-injected embryos at 8 hpf stained by HE. (**G** and **H**) Phalloidin staining shows reduced F-actin cytoskeleton around the cortical layer of dsRNA-stimulated cells. (**I** and **M**) TEM images showing robust mitophagy process in dsRNA-stimulated cells at 8 hpf. (**N**) Stacked columns show a strong increase in mitophagy in dsRNA-injected embryos. Scale bars: 500 μm for **B**, 50 μm for **E** and **F**, 20 μm for **G** and **H**, 500 nm for **I** and **J**, and 200 nm for **K** to **M**.

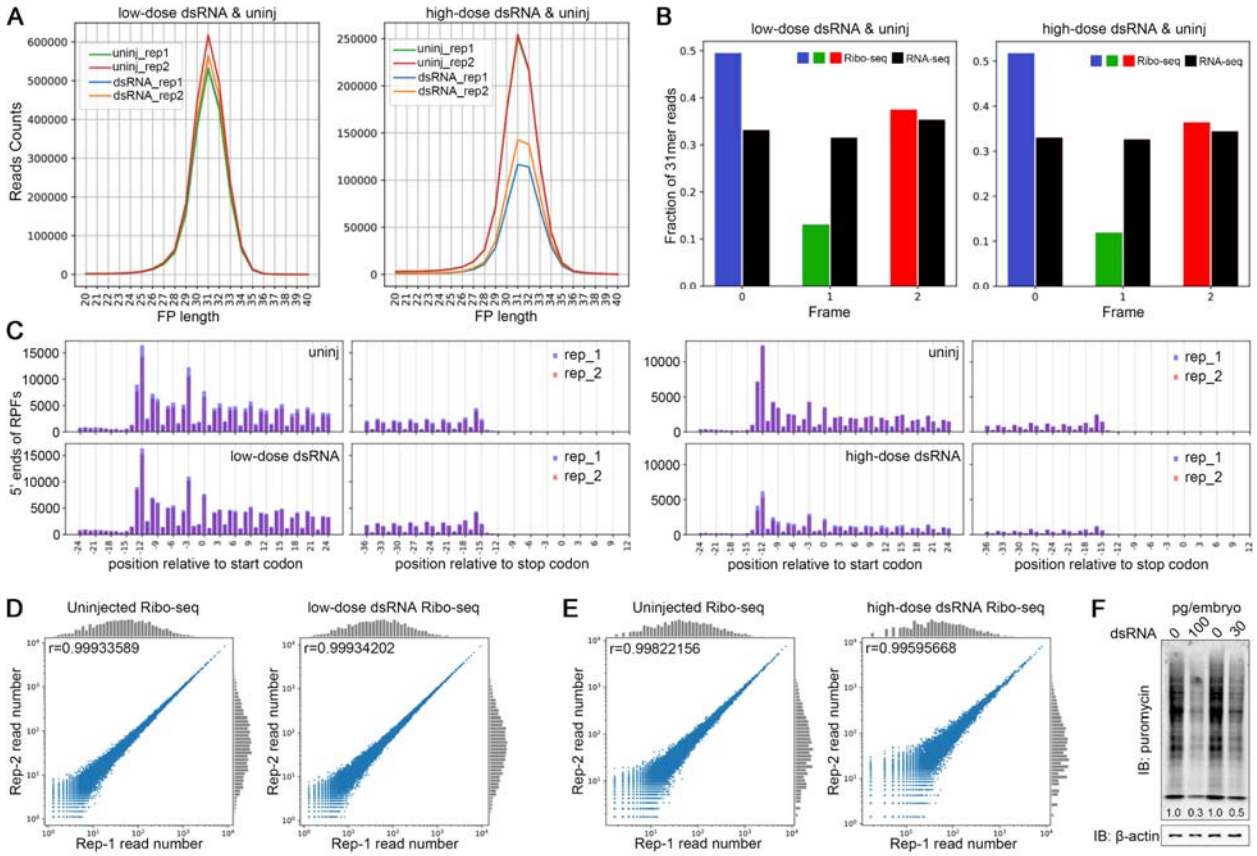

Supplementary Figure S2. Ribo-seq analysis of translation remodeling after dsRNA stimulation, related to Figure 2. (**A**) Read-length distribution of uniquely mapped RPFs. (**B**) Triplet periodicity of ribosome footprints revealed by reads aligning to the A-site of each reading frame but not by reads from RNA-seq. (**C**) Metagene analysis of ribosome profiling libraries, with 5' end of reads aligned to the start or stop codon. (**D** and **E**) Scatter plots illustrating reproducibility between replicates of Ribo-seq. (**F**) A representative puromycin incorporation experiment demonstrating the degree of reduction in global translation activity.

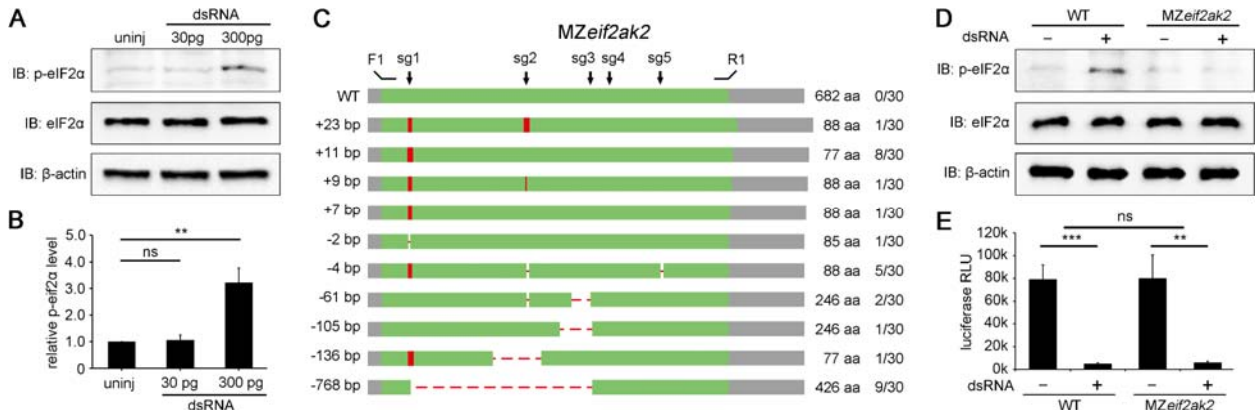

Supplementary Figure S3. PKR is not required for translation repression by dsRNA in early embryos, related to Figure 2. (**A** and **B**) Phosphorylation of eIF2α induced by high-dose of dsRNAs (300 pg/embryo). (**C**) Injection of Cas9 RNPs targeting the ORF of *eif2ak2* into 1-cell stage embryos. The CRISPants were raised to adults and crossed to produce MZ mutant embryos. ORF region of *eif2ak2* (green area) was amplified and sequenced from cDNAs of CRISPant-spawned embryos at 6 hpf. The result indicates the absence of WT alleles. sgRNA target sites are indicated by arrows. F1 and R1 are primers amplifying the ORF. UTRs are marked as grey. (**D**) Failure to phosphorylate eIF2α in MZ*eif2ak2* embryos by dsRNAs (300 pg/embryo). (**E**) Comparable dsRNA-induced translation blockage between WT and MZ*eif2ak2* embryos. Values are means ± SDs. ** $p<0.01$, *** $p<0.001$, ns, $p>0.05$, Student's *t*-test. ns in **E**, $p>0.05$, two-way ANOVA.

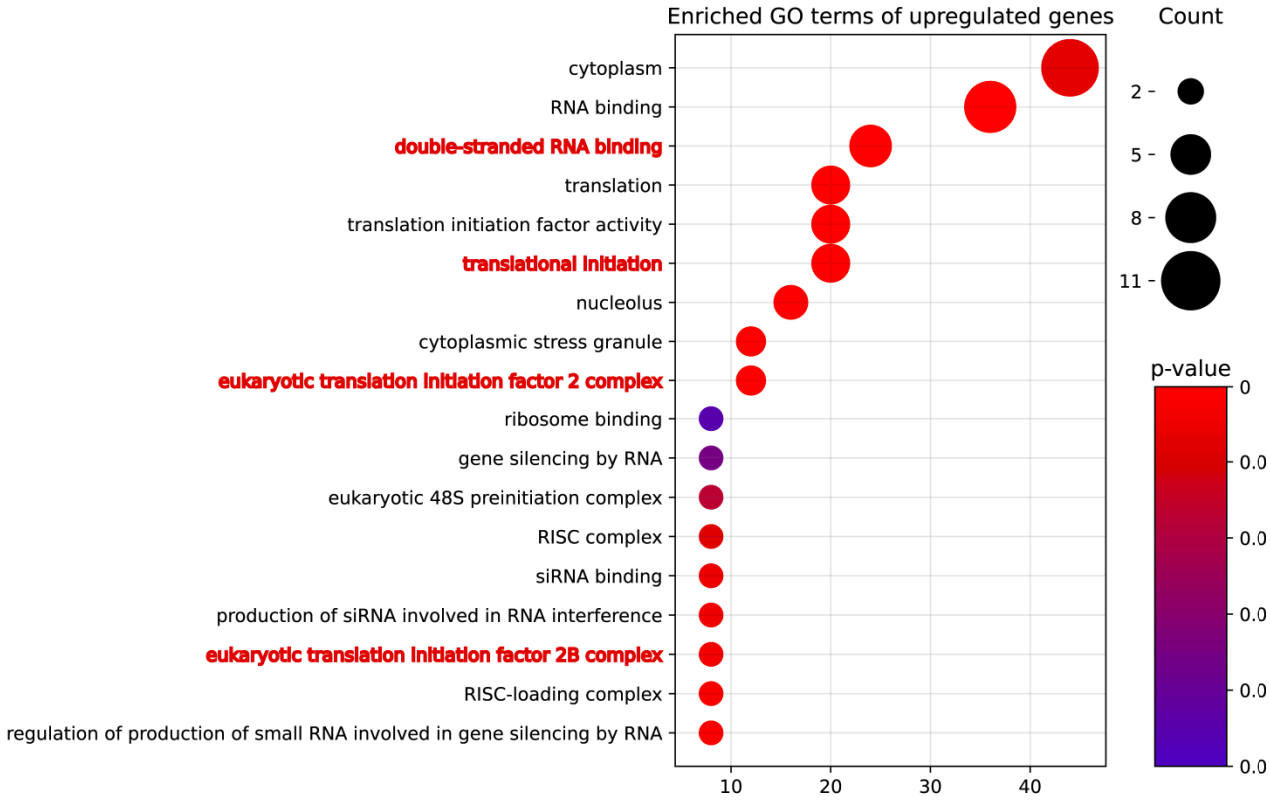

Supplementary Figure S4. Enriched GO terms of proteins specifically pulled down by dsRNAs, related to Figure 3. Red highlights dsRNA binding and translation-associated terms.

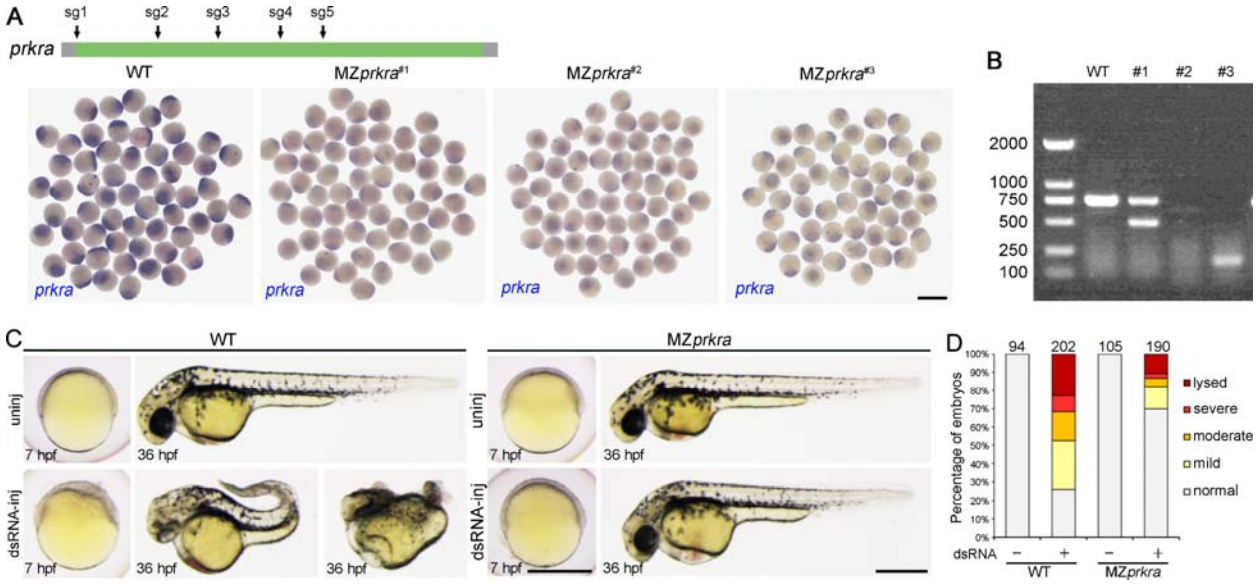

Supplementary Figure S5. *prkra* maternal mutants exhibit reduced sensitivity to dsRNA stimulation, related to Figure 4. (**A**) MZ*prkra* mutant embryos at the 1-cell stage from three independent F0 females, showing obvious non-sense mediated decay. (**B**) RT-PCR analysis of *prkra* CDS in MZ*prkra* embryos at the 4-cell stage. (**C**) Representative phenotypes caused by injection of dsRNAs (30 pg/embryo). (**D**) Histogram showing the reduced toxicity of dsRNAs in MZ*prkra* embryos. Scale bars: 1 mm for **A**, 500 μm for **C**.

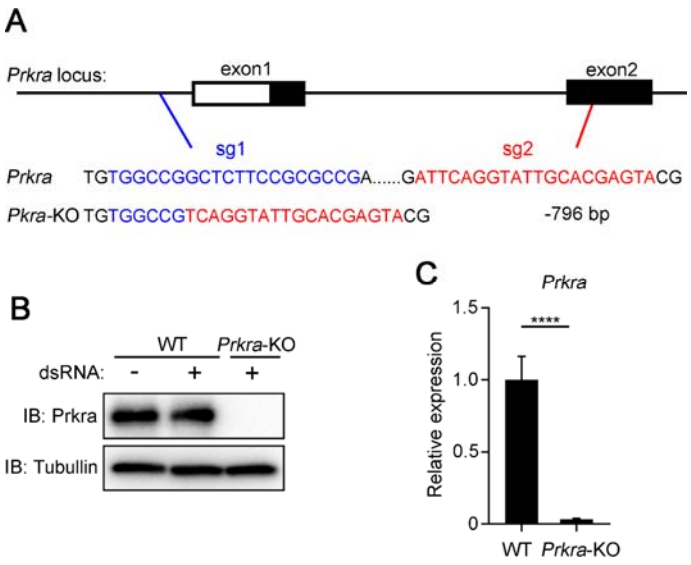

Supplementary Figure S6. Generation and verification of *Prkra* knockout mESCs, related to Figure 5. (**A**) Generation of *Prkra* deficient mESCs. (**B**) Absence of Prkra in *Prkra* knockout mESCs. (**C**) Severely reduced *Prkra* mRNA in the knockout cell line detected by qRT-PCR. Values are means ± SDs. **** $p<0.0001$, Student's *t*-test.

Supplementary Tables

Supplementary Table S1. Sequences of dsRNAs

dsRNA name	Sequence	Length (bp)
cas9 dsRNA1	GAUGGCAAAGGUUGACGAUAGCUUCUUUCAUAGACUGGAGGA GAGCUUCCUGGUCGAGGAGGACAAGAAGCACGAGAGACACCCC AUCUUCGGAAAUAUCGUGGACGAGGUGGCAUACCAUGAAAAG UAUCCUACCAUUUACCACCUGAGAAAAAAGCUGGUGGACAGCA CAGACAAGGCCGAUCUGAGACUGAUCUACCUGGCACUGGCCCA CAUGAUCAAAUUUAGAGGCCAUUUCCUGAUUGAAGGAGACCU GAACCCCGAUAACAGCGAUGUUGAUAAACUGUUCAUCCAACUG GUUCAGACCUAUAACCAACUGUUUGAGGAGAACCCUAUUAACG CCAGCGGAGUGGAUGCAAAGGCCAUCCUGAGCGCUAGACUGAG CAAAAGCAGAAGACUGGAAAAUCUGAUCGCCCAGCUGCCCGGC GAAAAAAAGAAUGGACUGUUCGGCAAUCUGAUUGCACUGAGC CUGGGACUGACACCUAACUUCAAGAGCAAUUUCGAUCUGGCUG AGGACGCCAAACUGCAGCUGAGCAAAGACACAUAUGAUGACGA CCUGGAUAACCUGCUGGCACAAAUUGGUGACCAAUACGCUGAC CUGUUCCUGGCUGCUAAGAAUCUGAGCGAUGCCAUUCUGCUGA GCGACAUCCUGAGAGUGAACACAGAGAUUACCAAGGCACCCCU GAGCGCAAGCAUGAUUAAGAGAUACGACGAGCACCACCAAGAU CUGACCCUGCUGAAGGCCCUGGUCAGACAACAACUGCCAGAGA AGUAUAAAGAAAUUUUCUUUGACCAAAGCAAGAACGGUUACG CUGGCUACAUUGACGGCGGUGCAAGCCAAGAGGAGUUCUAUAA GUUCAUUAAGCCAAUCCUGGAGAAAAUGGAUGGAACUGAGGA GCUGCUGGUUAAGCUGAAUAGAGAGGAUCUGCUGAGAAAACA AAGAACAUUCGACAACGGUAGCAUCCCACACCAGAUUCAUCUG GGUGAGCUGCACGCAAUUCUGA	1004
cas9 dsRNA2	UGAGCUGCACGCAAUUCUGAGAAGACAGGAAGACUUUUAUCCA UUCCUGAAGGACAACAGAGAAAAGAUCGAGAAGAUUCUGACA UUUAGAAUCCCCUACUACGUGGGACCUCUGGCUAGAGGCAAUA GCAGAUUCGCAUGGAUGACUAGAAAGAGCGAGGAGACAAUUA CCCCUUGGAACUUUGAAGAAGUGGUGGAUAAGGGAGCAAGCG CCCAAAGCUUCAUUGAGAGAAUGACAAACUUCGAUAAGAACCU GCCUAACGAGAAGGUUCUGCCCAAGCAUAGCCUGCUGUAUGAA UAUUUCACAGUGUACAACGAGCUGACAAAGGUCAAGUACGUCA CAGAGGGCAUGAGAAAGCCCGCCUUUCUGAGCGGAGAACAAAA GAAGGCUAUUGUUGACCUGCUGUUCAAGACCAACAGAAAAGU UACAGUUAAACAGCUGAAAGAGGACUACUUCAAAAAGAUUGA AUGUUUUGACAGCGUGGAAAUCAGCGGCGUUGAGGACAGAUU UAACGCUAGCCUGGGCACCUACCACGAUCUGCUGAAAAUCAUC AAAGAUAAGGACUUUCUGGACAACGAAGAAAACGAGGACAUU CUGGAAGACAUUGUGCUGACACUGACUCUGUUCGAAGAUAGA GAAAUGAUCGAGGAAAGACUGAAAACUUAUGCACAUCUGUUC GACGACAAAGUGAUGAAGCAACUGAAGAGAAGAAGAUACACU GGAUGGGGCAGACUGAGCAGAAAGCUGAUCAACGGAAUCAGA GACAAGCAAAGCGGAAAAACUAUUCUGGAUUUUCUGAAAAGC GACGGUUUCGCCAAUAGAAACUUCAUGCAACUGAUUCACGAUG ACAGCCUGACUUUCAAGGAGGAUAUUCAAAAGGCACAGGUGA GCGGCCAGGGCGAUAGCCUGCACGAACACAUCGCAAAUCUGGC CGGUAGCCCUGCCAUUAAGAAGGGCAUCCUGCAGACAGUGAAG	978

	GU	
cas9 dsRNA3	UCCUGCAGACAGUGAAGGUUGUUGAUGAACUGGUCAAGGUGA UGGGUAGACACAAGCCCGAGAAUAUUGUGAUCGAGAUGGCUA GAGAGAACCAAACAACACAAAAGGGACAGAAGAAUAGCAGAG AAAGAAUGAAAAGAAUUGAGGAGGGAAUCAAGGAGCUGGGUA GCCAGAUCCUGAAAGAACACCCUGUCGAGAAUACACAACUGCA AAACGAAAAGCUGUACCUGUACUACCUGCAAAAUGGCAGAGAC AUGUACGUGGACCAAGAGCUGGAUAUUAACAGACUGAGCGAC UACGAUGUCGACCACAUCGUGCCUCAAAGCUUCCUGAAGGAUG ACAGCAUCGACAAUAAAGUGCUGACUAGAAGCGACAAGAACAG AGGAAAAAGCGACAACGUGCCCAGCGAGGAAGUGGUUAAAAA GAUGAAGAACUACUGGAGACAGCUGCUGAAUGCCAAGCUGAUC ACACAAAGAAAAUUCGACAACCUGACCAAAGCCGAGAGAGGAG GUCUGAGCGAACUGGACAAGGCUGGAUUCAUUAAGAGACAAC UGGUUGAAACCAGACAGAUUACAAAGCACGUGGCUCAAAUCCU GGACAGCAGAAUGAAUACCAAAUAUGACGAGAACGACAAACU GAUUAGAGAGGUGAAGGUUAUUACUCUGAAGAGCAAACUGGU CAGCGACUUCAGAAAGGACUUCCAAUUCUACAAGGUGAGAGAG AUCAACAAUUACCACCACGCACACGACGCUUACCUGAACGCUG UGGUGGGCACAGCUCUGAUCAAAAAGUAUCCAAAACUGGAAA GCGAGUUUGUGUACGGUGACUAUAAAGUUUAUGAUGUGAGAA AAAUGAUCGCUAAGAGCGAGCAGGAGAUCGGAAAGGCUACAG CCAAGUAUUUCUUUUACAGCAACAUUAUGAACUUUUUCAAGAC UGAAAUCACCCUGGCAAACGGUGAGAUCAGAAAAAGACCACUG AUCGAAACAAAUGGCGAGACAGGCGAGAUCGUGUGGGAUAAG GGAAGAGACUUCGCUACCGUUAGA	1043
vps26c (*dscr3*)	UCUCUGGACAUCCGACUGAAGCGGGCGAAUAAAGUCUACCAUG AGGGGGAGCGUCUGUGUGGGCUGCUGGUGGUGGUCAGCAGAG ACCCGCUCCAGCAUCAGGGAGUGUCCCUCAGUCUGGAGGGUCU CGUCAACCUGCAGCUCAGCGCAAAGAGCGUCGGUGUGUUCGAG GCCUUCUACAACUCUGUCAAGCCCAUCCAGCUGGUGUCCAGCA CUAUGGAGGUGGCCAAGCCGGGGAAGGUUCCGGCGGGCAGGAC UGAGAUCCCCUUCGAGUUCCCUCUGCAGGCUAAAGGAAACAAG CAGCUGUACGAGACCUACCACGGCGUGUUCGUCAACAUCCAGU ACACACUCCGCUGUGACAUCAGACGCUCACUGCUGGCCAAAGA CCUCAGCAAGAGCUGCGAGUUCAUGGUGCACUGUCAGCCACAG AAGGCCAAGCUGCAGCCUAACCCAGUGGACUUCAGCAUCACAC CAGAGACUCUGCAGAACAUCAGAGAGCGGGCGUCUCUGCCGCG GUUCCUGAUCCGGGGUCAUCUGGACGCCACCUGCUGCUCGAUC ACGCGUCCCCUGAGCGGAGAGCUGGUGGUGGAGAACUCAGAGG	819

	UGCCCAUCAAGAGCAUCGAGCUGCAGCUGGUGCGGGUGGAGAC CUGCGGCUGUGCAGAGGGCUACGCCAGGGACGCCACAGAGAUC CAGAAUAUCCAGAUAGCAGAGGGUGACGUGUGUCACGGGCUCU CCAUCCCCAUCUACAUGGUGUUCCCCAGACUCUUCACCUGCCC CACGCUCGAGACCACCAACUUCAAAGUGGAGUUCGAGGUCAAC AUC	
Dengue virus	UUCCAUCUGACCACCCGAAACGGCGAACCCCAUAUGAUUGUGU CCAGGCAGGAGAAGGGCAAGAGUCUGCUGUUCAAAACUGAGG AUGGCGUGAACAUGUGCACCCUGAUGGCUAUGGACCUGGGGGA GCUGUGCGAAGAUACCAUCACAUACAAAUGUCCUUUCCUGAAG CAGAACGAGCCAGAAGACAUUGAUUGCUGGUGUAAUAGUACU UCAACCUGGGUGACAUAUGGGACUUGUACCACAACUGGAGAGC ACCGGAGAGAAAAGCGAUCUGUCGCACUGGUGCCACAUGUCGG AAUGGGACUGGAGACACGCACUGAAACCUGGAU	332
Ebola virus	AUGACAACUAGAACAAAGGGCAGGGGCCAUACUGCGGCCACGA CUCAAAACGACAGAAUGCCAGGCCCUGAGCUUUCGGGCUGGAU CUCUGAGCAGCUAAUGACCGGAAGAAUUCCUGUAAGCGACAUC UUCUGUGAUAUUGAGAACAAUCCAGGAUUAUGCUACGCAUCCC AAAUGCAACAAACGAAGCCAAACCCGAAGACGCGCAACAGUCA AACCCAAACGGACCCAAUUUGCAAUCAUAGUUUUGAGGAGGUA GUACAAACAUUGGCUUCAUUGGCUACUGUUGUGCAACAACAAA CCAUCGCAUCAGAAUCAUUAGAACAACGCAUUAC	335
HIV	GAACAAGCCCCAGAAGACCAAGGGCCACAGAGGGAGCCACACA AUGAAUGGACACUAGAGCUUUUAGAGGAGCUUAAGAAUGAAG CUGUUAGACAUUUUCCUAGGAUUUGGCUCCAUGGCUUAGGGCA ACAUAUCUAUGAAACUUAUGGGGAUACUUGGGCAGGAGUGGA AGCCAUAAUAAGAAUUCUGCAACAACUGCUGUUUAUCCAUUUC AGAAUUGGGUGUCGACAUAGCAGAAUAGGCGUUACUCAACAG AGGAGAGCAAGAAAUGGAGCCAGUAGAUCC	285
Influenza A virus	AUGGCGUCCCAAGGCACCAAACGGUCUUACGAACAGAUGGAGA CUGAUGGGGAACGCCAGAAUGCAACUGAAAUCAGAGCAUCCGU CGGAAGAAUGAUUGGUGGAAUUGGGCGAUUCUACAUCCAAAU GUGCACCGAGCUUAAACUCAAUGAUUAUGAGGGACGACUGAUC CAGAACAGCUUGACAAUAGAGAGAAUGGUGCUCUCUGCUUUU GAUGAGAGGAGGAAUAAAUAUCUGGAAGAACAUCCCAGCGCG GGGAAAGAUCCUAAGAAAACUGGAGGACCCAUAUACAAGAGA GUAGAUGGAAAGUGGGUGAGGGAACUCGUCCUU	330
SARS-CoV-2 virus	UGCCACUAGUCUCUAGUCAGAGAGUCCAACCAACAGAAUCUAU UGUUAGAUUUCCUAAUAUUACAAACUUGUGCCCUUUUGGUGA AGUUUUUAACGCCACCAGAUUUGCAUCUGUUUAUGCUUGGAAC AGGAAGAGAAUCAGCAACUGUGUUGCUGAUUAUUCUGUCCUA UAUAAUUCCGCAUCAUUUUCCACUUUUAAGUGUUAUGGAGUG UCUCCUACUAAAUUAAAUGAUCUCUGCUUUACUAAUGUCUAUG CAGAUUCAUUUGUAAUUAGAGGUGAUGAAGUCAGACAAAUCG CUCCAGGGCAAACUGGAAAGAUUGCUGAUUAUAAUUAUAAAU UACCAGAUGAUUUUACAGGCUGCGUUAUAGCUUGGAAUUCUA ACAAUCUUGAUUCUAAGGUUGGUGGUAAUUAUAAUUACCGGU	645

	AUAGAUUGUUUAGGAAGUCUAAUCUCAAACCUUUUGAGAGAG AUAUUUCAACUGAAAUCUAUCAGGCCGGUAGCACACCUUGUAA UGGUGUUCAAGGUUUUAAUUGUUACUUUCCUUUACAAUCAUA UGGUUUCCAACCCACUAAUGGUGUUGGUUACCAACCAUACAGA GUAGUAGUACUUUCUUUUGAACUUCUACAUGCACCAGCAACUG UUUGUGGAC	
Tilapia lake virus	AUGAGUGUGGCAGAUUAUUUGUCAAGUGACAGUGACUCGGGG GCUGAGAGCUCAGGAUGUUUAGUACUAAGAAGUCGGAAGAUC AAGAAGGGCAAGAAAGCUGCUUCAAAGAAGCGAAGUUGGAAG AAUGAAAGGUAUGGUGCUGACGAGAGCGGUGAAGAUAAUAUA GAGUGGGGUGACGAAGUCGACCUCGAGAUGGACGACUGUGAU UCUGCAAUCCCAGAGUGGGCUAGGGUUGAUUUCAAUCCCAAAA ACAGAAGGGACAGAGAGGAUGAUGGGCAGAGUGACCUAUCUC GAUUUUCCGAAGAUUUCGGAAAGAAGUCUCUUGACGUGCAGU CUUAG	342
Zika virus	GACGUGGGGUGCUCAGUGGACUUCUCAAAAAAGGAAACGAGA UGUGGCACGGGGGUAUUCAUCUAUAAUGAUGUUGAAGCCUGG AGGGACCGGUACAAGUACCAUCCUGACUCCCCCCGCAGAUUGG CAGCAGCAGUCAAGCAGGCCUGGGAAGAGGGGAUCUGUGGGA UCUCAUCCGUUUCAAGAAUGGAAAACAUCAUGUGGAAAUCAG UAGAAGGGGAGCUCAAUGCUAUCCUAGAGGAGAAUGGAGUUC AACUGACAGUUGUUGUGGGAUCUGUAAAAAACCCCAUGUGGA GAGGUCCACAAAGAUUGCCAGUGCCUGUGAAUGAGC	331
Biotinylated-dsRNA (pull down)	bioUin- GAUUGUUUAGGAAGUCUAAUCUCAAACCUUUUGAGAGAGAUA UUUCAACUGAAAUCUAUCAGGCCGGUAGCACACCUUGUAAUGG UGUUCAAGGUUUUAAUUGUUACUUUCCUUUACAAU	120
dsRNA (EMSA)	UCCUAGGAUUUGGCUCCAUGGCUUAGGGCAACAUAUCUAUGAA ACUUAUGGGGAUACUUGGGCAGGAGUGGAAGCCAUAAUAAGA AUUCUGCAACAACUGCUGUUUAUCCAUUUCAGAAUUGGGUGUC GACAUAGCAGA	139

Supplementary Table S2. Primers used in this study

Usage	Primer name	Sequence 5'-3'	note
Synthesis of the three dsRNA segments from the *cas9* sequence	*cas9*-1 sp6-F	ATTTAGGTGACACTATAGAGATGGCAAAGGTTGACGA	
	cas9-1-R	TCAGAATTGCGTGCAGCTCA	
	cas9-1-F	GAGATGGCAAAGGTTGACGA	
	cas9-1-sp6-R	ATTTAGGTGACACTATAGATCAGAATTGCGTGCAGCTCA	
	cas9-2 sp6-F	ATTTAGGTGACACTATAGATGAGCTGCACGCAATTCTGA	
	cas9-2-R	ACCTTCACTGTCTGCAGGAT	
	cas9-2-F	TGAGCTGCACGCAATTCTGA	
	cas9-2-sp6-R	ATTTAGGTGACACTATAGACCTTCACTGTCTGCAGGAT	
	cas9-3 sp6-F	ATTTAGGTGACACTATAGATCCTGCAGACAGTGAAGGT	
	cas9-3-R	TCTAACGGTAGCGAAGTCTC	
	cas9-3-F	ATCCTGCAGACAGTGAAGGT	
	cas9-3-sp6-R	ATTTAGGTGACACTATAGATCTAACGGTAGCGAAGTCTC	
Synthesis of biotin-labeled dsRNAs from the HIV1-Vpr sequence	HIV-140-F	TCCTAGGATTTGGCTCCATG	
	HIV-140-R	TCTGCTATGTCGACACCCAA	
	HIV-140-sp6 F	ATTTAGGTGACACTATAGTCCTAGGATTTGGCTCCATG	
	HIV-140-sp6 R	ATTTAGGTGACACTATAGTCTGCTATGTCGACACCCAA	
qPCR primers	*gapdh* qPCR-F	TTGCCGTTCATCCATCTTTG	
	gapdh qPCR-R	TGCTGTAACCGAACTCATTGTC	
	SVCV-F	TACACGGAAATCTACCTAACACA	SVCV quantification
	SVCV-R	TTCAGCTGCATGGCAGATCCATCCA	
Primers for genotyping CRISPant or mutants	p150-*eif2ak2*-fwd	TGGCAAAGAATTCCTCGACGGGACAGAAGTTTCCTGATG	
	p150-*eif2ak2*-rev	CACCATGGTGGCGACCGGTGTGATTCATCTGCTCTGGG	
	p150200-*prkra*-F	GGCAAAGAATTCCTCGACGGCAGAAGTAATGGCTGATTC	
	p150200-*prkra*-R	ACCATGGTGGCGACCGGTGGGAATTACGCAAGCTTTCCAC	
	MS-*Prkra* sg1-F	CTGAGCACTGTGGCAAAGTGGAGC	
	MS-*Prkra* sg1-R	CACAGCAATCAAGAGAAGTGTGGATCTG	
	MS-*Prkra* sg2-F	CAAGATGATAACAGCTAAGCCTGGG	
	MS-*Prkra* sg2-R	GTTATGTCACCAACGGTTACTCTG	
Primers	*eif2ak2*-sg1	taatacgactcactataGGGCACTCACAGTGATGAACgttttag	

for sgRNA synthesis		agctagaa	
	eif2ak2-sg2	taatacgactcactataGGGACTTACATTGGGTTGTGgttttaga gctagaa	
	eif2ak2-sg3	taatacgactcactataGGGCCACTAGTCCTGTAAGTgttttaga gctagaa	
	eif2ak2-sg4	taatacgactcactataGGGTTTGGTACCTTCATGTCgttttaga gctagaa	
	eif2ak2-sg5	taatacgactcactataGGTCCGCTACTTCTCGTCTTgttttaga gctagaa	
	prkra-sg1	taatacgactcactataGGGGAGCCATTGTGACACTGgttttag agctagaa	
	prkra-sg2	taatacgactcactataGGGCCGAGGATCCACAAAAAgttttag agctagaa	
	prkra-sg3	taatacgactcactataGGGAGAAGCGTCCAATCCTGgttttag agctagaa	
	prkra-sg4	taatacgactcactataGGCCTGCCGTCTGGAGGGACgttttag agctagaa	
	prkra-sg5	taatacgactcactataGGGATCTTCTGAGATCACGTgttttaga gctagaa	
	tail primer	AAAAGCACCGACTCGGTGCCACTTTTTCAAGTTG ATAACGGACTAGCCTTATTTTAACTTGCTATTTCT AGCTCTAAAAC	
sgRNA sequences of mouse *Prkra*	MS-*Prkra*-sgRNA1	TGGCCGGCTCTTCCGCGCCG	To insert target sequences into pSpCas9(BB)-2A-GFP (PX458)
	MS-*Prkra*-sgRNA2	ATTCAGGTATTGCACGAGTA	
Synthesis of Prkra or truncated variants	pET Duet-*prkra*-F	ACTTTAAGAAGGAGATATACATGGCTGATTCAAA TGTC	Clone sequences of *prkra* orf into pET-Duet vector
	pET Duet-*prkra*-R	TTTACCAGACTCGAGGGTACTTAGTGGTGATGAT GGTGATGGTGTTTGCTGGCCACCATCT	
	pET Duet-*prkra*-nest F	AGACGGGCAGAAGTAATGG	
	pET Duet-*prkra*-nest R	ACCCCAGACCTGCTGTTAG	
	pETduet-*prkra* ΔDSRM1-F	AGGATCCACAATAATAGACCAGAGAGACAAC	Clone sequences of *prkra* truncated ORF into pET-Duet vector.
	pETduet-*prkra* ΔDSRM1-R	GGTCTATTATTGTGGATCCTCGGCCTTTGC	
	pETduet-*prkra* ΔDSRM2-F	CGGCAGCTCCGGATCTTCTGAGATCACGTG	
	pETduet-*prkra* ΔDSRM2-R	CAGAAGATCCGGAGCTGCCGGATCCTGTTT	
	pETduet-*prkra* ΔDSRM3-F	TGGAGTGACCAAACACCATCACCATCATCA	
	pETduet-*prkra* ΔDSRM3-R	GATGGTGTTTGGTCACTCCAGAGCCATGAC	

Primers for amplifying DNA templates used for the synthesis of probes for northern blotting	*GFP*-NB probe-F	ATGGTGAGCAAGGGCGAGGA	
	GFP-NB probe-R	TAATACGACTCACTATAGCTTGTACAGCTCGTCCATGC	